



## Relative paleointensity stack during the last 250 kyr in the northwest Pacific

Y. Yamamoto,<sup>1,2</sup> T. Yamazaki,<sup>1</sup> T. Kanamatsu,<sup>3</sup> N. Ioka,<sup>4</sup> and T. Mishima<sup>5</sup>

Received 28 April 2006; revised 6 September 2006; accepted 25 September 2006; published 26 January 2007.

[1] We have conducted a paleomagnetic study of 10 sediment cores recovered from the northwest Pacific. The purpose is to establish a regional paleointensity stack during the last 250 kyrs (NOPAPIS-250) for global coverage of paleointensity data as well as a regional reference for paleointensity-assisted stratigraphy. In the studied cores, reductive dissolution of magnetite appears to have occurred mainly in glacial periods. Such horizons accompany large decreases in S-ratio ( $S_{-0.3T} = (1 - \text{IRM}_{-0.3T}/\text{SIRM})/2$ ) as low as 0.90. The sediments are also intercalated by frequent volcanic ash layers. Prerequisites for reliable relative paleointensity estimation are not satisfied at these horizons. We rejected unsuitable data by quantitative criteria based on S-ratio and saturation isothermal remanent magnetization (SIRM) and constructed the NOPAPIS-250 curve from the remaining data. In the construction of the curve, we chose IRM as a normalizer because acquisitions of anhysteretic remanent magnetization (ARM) are considered to be influenced by magnetic interactions among magnetic grains in the northwest Pacific sediments. Relative intensity variation of the NOPAPIS-250 gives a standard deviation that is 33% of the average, if the normal distribution is assumed. The NOPAPIS-250 curve generally shows similar variation patterns compared with other high-resolution records reported from other regions: many paleointensity lows are recognized in common. Six out of the nine lows can be correlated with reported excursions in literature.

**Citation:** Yamamoto, Y., T. Yamazaki, T. Kanamatsu, N. Ioka, and T. Mishima (2007), Relative paleointensity stack during the last 250 kyr in the northwest Pacific, *J. Geophys. Res.*, 112, B01104, doi:10.1029/2006JB004477.

### 1. Introduction

[2] In the last decade, relative paleointensity studies have progressed significantly. As a result, the master curve of geomagnetic field variations was obtained for the last 800 kyrs (Sint-800 [Guyodo and Valet, 1999]). Further efforts have been made to construct longer time series for an older era and high-resolution stacks for a younger period. For the former time series, Valet *et al.* [2005] and Yamazaki and Oda [2005] recently reported new relative paleointensity stacks spanning the last 2000 and 3000 kyrs, respectively (Sint-2000 and EPAPIS-3Ma). They are characterized by quasi-periodic paleointensity lows which may be correlated with both known and unknown geomagnetic excursions. For the latter, Laj *et al.* [2000] compiled six relative paleointensity records from the north Atlantic Ocean to produce a new stacked curve for the last 75 kyr (NAPIS-75). Stoner *et al.*

[2002] integrated five records from the sub-Antarctic south Atlantic into a stacked curve covering the last 80 kyr (SAPIS). A 400 kyr stack based on eight sediment cores from the Portuguese margin (northeast Atlantic) was reported by Thouveny *et al.* [2004]. These records highlight high-frequency lows and highs in paleointensity, which cannot be recognized in the previous master curve of the Sint-800.

[3] New high-resolution stacks are required for other regions because the geomagnetic field is a global phenomenon. Many existing high-resolution stacks have been obtained from the north Atlantic [e.g., Laj *et al.*, 2000; Thouveny *et al.*, 2004]. It is important to construct a new stack in the northwest Pacific, almost the opposite side of the north Atlantic. There has been no such stack reported from this region, and it is required to make efforts for constructing a new stack in such areas for global coverage of paleointensity data. A new stack will be useful as a high-resolution chronology tool because water depths of the northwest Pacific are mostly below the calcium carbonate compensation depth (CCD) and oxygen isotope stratigraphy is usually not applicable for this region. Recent studies have revealed that high-resolution paleointensity records have great potential for a global correlation of marine sediments in the late Pleistocene [e.g., Stoner *et al.*, 2000].

[4] In this article, we focus on the northwest Pacific and construct a new high-resolution paleointensity stack for the

<sup>1</sup>Geological Survey of Japan, AIST, Tsukuba, Japan.

<sup>2</sup>Now at Geomagnetism Laboratory, University of Liverpool, Liverpool, UK.

<sup>3</sup>Institute for Research on Earth Evolution, Japan Agency for Marine-Earth Science and Technology, Yokosuka, Japan.

<sup>4</sup>The General Environmental Technos Co., Ltd., Osaka, Japan.

<sup>5</sup>Center for Advanced Marine Core Research, Kochi University, Kochi, Japan.

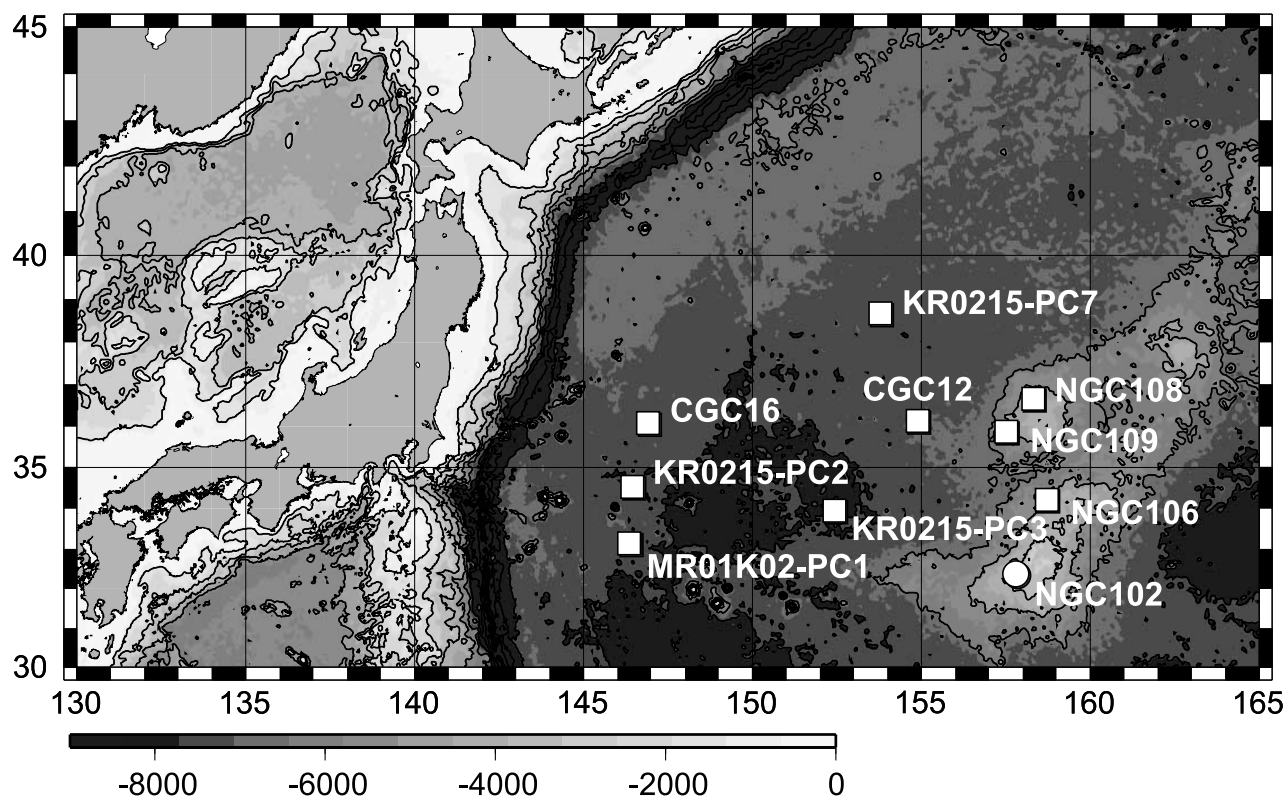


**Figure 1.** Simplified bathymetry of the northwest Pacific and location of coring sites.

last 250 kyr (NOPAPIS-250) from ten sediment cores. The present cores are intercalated by frequent volcanic ash layers. They offer precise calibration points in age because some of them are well-known dated widespread tephra around Japan. They also provide reliable tie points for stacking. However, prerequisite for reliable relative paleointensity, rock magnetic homogeneity, do not stand for throughout the present cores. In the construction of NOPAPIS-250 curve, we have made an attempt to exclude data from such nonhomogeneous horizons.

## 2. Geological Setting and Core Sample

[5] The northwest Pacific Ocean is one of the oldest ocean basins. Owing to Jurassic to Cretaceous ages of its seafloor, water depths of the ocean (about 5000–6000 m) are generally deeper than the CCD. However, there is a broad plateau of the Shatsky Rise rising to depths of 2500–3500 m with an area of about 75,000 km<sup>2</sup>. Studies of marine magnetic anomaly suggested that the rise was formed at a ridge-ridge-ridge type triple junction during the Late Jurassic to the Early Cretaceous [Nakanishi *et al.*, 1989, 1999; Sager and Han, 1993]. Biological productivity is relatively high in this area [Berger, 1989].

[6] Six gravity and four piston cores were collected in the northwest Pacific Ocean (Figure 1 and Table 1). Since a gravity core of NGC102 showed low sedimentation rate compared with the other nine cores, it was only used as a reference of age model.

[7] Gravity cores of NGC102, NGC106, and NGC108 were acquired from the Shatsky Rise during the R/V Hakurei-Marū NH95-1 cruise. They mainly consist of

calcareous nannofossil ooze [Ioka *et al.*, 1997] because water depths of the coring sites are shallower than the CCD. They are also intercalated by several volcanic ash layers. For the cores of NGC102 and NGC108, oxygen isotope records were reported by Kawahata *et al.* [1999] (NGC102, the last 300 kyr) and Maeda *et al.* [2002] (NGC108, the last 180 kyr). At 274 cm in depth of NGC102, the age was estimated to be 0.26 Ma based on calcareous nannofossils *E. huxleyi*. [Tanaka, 1997]. He concluded that the ages of the lowermost part of NGC106 and NGC108 are younger than 0.26 Ma. These estimations are consistent with the age models from the oxygen isotope records. Other cores, NGC109, CGC12, and CGC16 were obtained from sites with depths below the CCD during the R/V Hakurei-Marū NH95-1 and Hakurei-Marū No.2 NH99 cruises. They are mainly composed of pelagic clay intercalated by several volcanic ash layers [Ioka *et al.*, 1997; Fukuhara *et al.*, 2001].

[8] Piston cores of KR0215-PC2, KR0215-PC3, and KR0215-PC7 were recovered during the R/V Kairei KR02-15 cruise. They consist of pelagic clay and are intercalated by frequent volcanic ash layers [Irina *et al.*, 2003]. Another core of MR01K02-PC1 was retrieved during the R/V Mirai MR01-K02 cruise. This core is also composed of pelagic clay with intercalated volcanic ash layers [Yamamoto and Kanamatsu, 2002]. Saganuma *et al.* [2006] studied tephro-stratigraphy of these piston cores. On the basis of mineral composition, shape and major chemical composition of volcanic glasses, and stratigraphy, they found three widespread tephra around Japan and other three tephra correlative with each other but unknown origin (Table 2, boldface). As for the former tephra, eruption ages

**Table 1.** Sediment Cores Used in This Study<sup>a</sup>

Core	Position		Depth, m	Length, m	Number		Dep. Rate, cm/kyr	Interval, kyr
					Collected	Retained		
KR0215-PC2	34°29.1'N	146°30.0'E	5936	11.7	508	315	3.8	0.62
KR0215-PC3	33°54.0'N	152°28.2'E	5970	18.8	802	681	5.4	0.44
KR0215-PC7	38°37.7'N	153°50.1'E	5750	17.6	694	481	4.9	0.48
MR01K02-PC1	33°05.0'N	146°25.0'E	5758	11.5	510	405	4.2	0.56
NGC102	32°19.8'N	157°51.0'E	2612	3.3	134	-	1.3	1.9
NGC106	34°09.9'N	158°45.1'E	3713	6.4	262	181	2.6	0.94
NGC108	36°36.9'N	158°20.9'E	3390	6.5	266	127	2.6	0.94
NGC109	35°50.1'N	157°33.5'E	4530	6.5	265	154	4.7	0.52
CGC12	36°05.0'N	154°56.4'E	5596	4.4	189	127	3.2	0.73
CGC16	36°01.8'N	146°58.0'E	5667	4.2	188	129	4.0	0.59

<sup>a</sup> Number collected, number of discrete samples taken from each core; Number retained, number of samples used for the paleointensity stack; Dep. rate, estimated average deposition rate based on the age model of NGC102 [Kawahata *et al.*, 1999]; Interval, estimated time interval between samples.

have been estimated to be 86–90 ka (Aso-4) and 240 ka (Ata-Th) [Oba, 1991; Machida and Arai, 2003]. Since magnetic susceptibilities of these cores show similar variation patterns (section 3.1), Suganuma *et al.* [2006] tied these records based on the magnetic susceptibility as well as the tephro-stratigraphy. They compared the tied records to the susceptibility curve of NGC102, age model of which was already reported by Kawahata *et al.* [1999], and constructed age models. According to their results, sedimentation rates are estimated to be 1–8 cm/kyr, varying with time and place.

[9] Samples for paleomagnetic measurements were taken on board sequentially from split core sections using discrete plastic cubic capsules of 10 cm<sup>3</sup> (NGC cores) or 7 cm<sup>3</sup> (other cores). They were hermetically sealed and stored in refrigerators. Details of the samples are referred to in Table 1.

### 3. Magnetic Measurements and Results

[10] Magnetic measurements were carried out for separate sample sets. We call here “A set,” “B set,” “C set,” and “D set.” The A set consists of samples from the cores of NGC102, NGC106, and NGC109; the B set is composed of those from NGC108; the C set is those from CGC12, CGC16, and KR0215-PC7; and the D set is those from MR01K02-PC1, KR0215-PC2, and KR0215-PC3.

#### 3.1. Magnetic Susceptibility

[11] For the A and B set samples, low-frequency (0.47 kHz) magnetic susceptibility was measured on all discrete samples with a Bartington MS2 susceptometer. Susceptibility measurements for the C and D sets were performed on all discrete samples by an AGICO Kappa-bridge KLY-3 with an operating frequency of 875 Hz. The results are presented in Figures 2 and 3 for the piston and gravity cores, respectively. In Figure 2 the oxygen isotope records of NGC102 [Kawahata *et al.*, 1999] and SPECMAP [Imbrie *et al.*, 1989; McIntyre *et al.*, 1989] are also shown for comparison. Susceptibility changes might appear to lead the oxygen isotope signal. It is probably due to low resolution of the oxygen isotope record of NGC102, although it might show a particular environmental change of this area.

[12] The resultant susceptibility curves show similar short-cycle peaks and troughs among the records. The

curves are also generally analogous to curves of oxygen isotope records (e.g., SPECMAP [Imbrie *et al.*, 1989; McIntyre *et al.*, 1989]) low-high periodicity of ~100 kyr is recognized not only in the isotope records but also in the susceptibility curves. These characteristics were already reported for the piston cores [Suganuma *et al.*, 2006]. In the same way as Suganuma *et al.* [2006], we can tie these records based on the susceptibilities. First, we found prominent troughs probably relevant to glacial maxima (~20, 140, and 260 ka; dashed lines indicated as b, 3, 6, and 8 in Figures 2 and 3). Second, we could pick up several characteristic troughs and peaks between the prominent troughs (dotted lines in Figures 2 and 3). It is reasonable to consider that these horizons are isochronous among the cores. The tie points indicated by single numbers (1–8) or capital alphabets (A–F, volcanic ash layers) in the piston cores are the same as those in the work of Suganuma *et al.* [2006]. The identified ash layers in the work of Suganuma *et al.* (boldface in Table 2) are displayed as gray lines in Figure 2. Other tie points of the piston cores and all tie points of the gravity cores are newly presented in this study. Depths of the tie points are listed in Table 2.

#### 3.2. Natural Remanent Magnetization

[13] For the A set samples, every other discrete samples were subjected to blanket alternating field (AF) demagnetization of 15 mT, after stepwise AF demagnetization on several pilot samples per each core. These demagnetizations were done by an AF demagnetizer of DEM-8601 (Natsuhara Giken) and natural remanent magnetizations (NRMs) were measured by a cryogenic magnetometer of ScT-113. The other half of the samples from the A set were subjected to progressive AF demagnetization up to 80 mT by a cryogenic magnetometer system with an inline static AF demagnetizer (2G Enterprises model 760R). For the B, C, and D sets, NRM measurements were performed on all discrete samples by the same cryogenic magnetometer systems. Progressive AF demagnetization was conducted up to 40–80 mT.

[14] Almost all samples showed a single stable component after removals of secondary remanences at 10–20 mT. About 90% of the samples yielded maximum angular deviation (MAD) angles smaller than 5° in the principal component analysis [Kirschvink, 1980], indicating stable nature of the primary components (Figure 4a). Rest 10% of

Table 2. Depths of the Tie Points<sup>a</sup>

Tie Points	tephra	Age, ka	NGC102, m	NGC106, m	NGC108, m	NGC109, m	CGC12, m	CGC16, m	KR0215-PC2, m	KR0215-PC3, m	KR0215-PC7, m	MR01K02-PC1, m
a		11	0.18	0.13	0.26	0.06	0.19	0.06	-	0.38	-	0.13
b		22	0.34	0.47	0.36	0.28	0.49	0.34	-	0.75	-	0.55
c		32	0.46	-	1.14	0.67	0.85	0.98	-	1.79	-	-
d		44	0.60	1.08	1.57	1.40	1.21	1.60	1.02	2.67	-	1.78
1		61	0.82	1.59	2.40	2.13	1.91	2.31	1.37	3.48	2.52	2.23
A	Aso-4	88	-	1.93	3.26	3.03	2.76	3.23	2.24	4.44	3.58	3.33
B	On-Pml	98	-	-	-	-	2.89	3.37	2.44	4.67	5.13	3.64
2		124	1.25	-	4.11	3.28	3.62	3.81	3.26	5.29	6.28	4.75
3		142	1.48	2.76	4.77	3.89	4.21	-	3.72	6.12	7.09	5.53
3a		149	-	-	5.21	4.16	-	-	4.18	6.65	7.58	5.91
C	Unknown-1	159	-	3.52	5.57	5.06	-	-	4.84	7.44	8.92	6.37
4		166	1.91	3.83	5.85	5.53	-	-	5.12	8.01	9.94	6.72
4a		180	-	-	6.34	-	-	-	-	8.62	-	-
5		188	2.17	4.28	-	5.77	-	-	5.91	8.96	10.46	7.52
5a		201	-	-	-	6.25	-	-	6.14	9.62	-	-
D	Unknown-2	219	2.34	4.71	-	-	-	-	6.74	10.88	10.46	8.56
E	Unknown-3	230	-	-	-	-	-	-	7.24	10.88	-	9.23
F	Ata-Th	240	-	-	-	-	-	-	7.36	11.25	11.32	9.57
6		258	2.67	5.23	-	-	-	-	7.55	11.63	12.20	9.94
7		288	3.11	-	-	-	-	-	8.92	12.96	13.24	-
8		-	-	-	-	-	-	-	10.09	15.65	16.01	-

<sup>a</sup> Boldface represents the identified volcanic ash layers in the work of Suganuma *et al.* [2006]. Other tie points are picked on the basis of similarity in the susceptibility variations. Ages are referred from the oxygen isotope stratigraphy of NGC102 (last 300 kyr [Kawahata *et al.*, 1999]), except for the Aso-4 (A) and Ata-Th (F) layers.

the samples showed more noisy demagnetization behavior, but many of them still seem to give meaningful paleodirections (Figure 4b). Paleodirections and MAD values are illustrated for all cores in the auxiliary material<sup>1</sup>.

### 3.3. Anhyseretic and Isothermal Remanent Magnetizations

[15] For every other sample of the A set, anhysteretic remanent magnetization (ARM) was given by a 100  $\mu$ T biasing field with a smoothly decreasing AF field of 100 mT. The remanences were measured after the ARM acquisition and demagnetization at AF field of 15 mT. ARMs of the samples from the B, C, and D sets were imparted by a DC field of 100  $\mu$ T with the maximum AF field of 80 mT. Progressive AF demagnetization was performed on these ARMs and remanences were measured at each step.

[16] After demagnetizing the ARMs, experiments of isothermal remanent magnetization (IRM) acquisition were conducted. A pulse magnetizer of 2G model 660 was used for the acquisitions of the samples from the A, B, and C sets, whereas that of MMPM-9 (Magnetic measurements) was for the D set samples. In the experiment, an IRM of 2.5 T was imparted first (except for MR01K02-PC1, which was at 1 T). This is regarded as saturation IRM (SIRM). Then, the remanences were demagnetized at AF of 20 and 30 mT, and an IRM of 0.3 T was subsequently given in the direction opposite to SIRM ( $IRM_{-0.3T}$ ). The IRMs were measured using spinner magnetometers of SMM-85 or ASPIN (Natsuhara-Giken). S-ratios ( $S_{-0.3T}$ ) were calculated as  $S_{-0.3T} = (1 - IRM_{-0.3T}/SIRM)/2$ , following the definition of Bloemendal *et al.* [1992].

[17] Resultant S-ratios are presented in Figures 5 and 6 for the piston and gravity cores, respectively. They show synchronous variations in general if the tie points are considered. In particular, large decreases reaching  $\sim 0.90$  are observed at several horizons (dashed lines indicated as b, 3, 6, and 8), which correspond to glacial maxima (section 3.1). These observations support that the present choices of the tie points (section 3.1) are appropriate. Except for these horizons, the S-ratios mostly range from 0.95 to 0.98.

## 4. Construction of Relative Paleointensity Stack

[18] For a reliable estimation of relative paleointensity, rock magnetic homogeneity is an indispensable prerequisite. The cores, however, show large decreases of the S-ratios reaching as low as  $\sim 0.90$  at several horizons (Figures 5 and 6). In this section we attempt to exclude the remanence data from inhomogeneous horizons. A relative paleointensity stack is constructed from the remaining data. In the construction of the stack, we also discuss our choice of a normalizer since proper normalization for efficiency of DRM (depositional remanent magnetization) acquisition is another important prerequisite for the reliable relative paleointensity estimation [e.g., Tauxe, 1993].

### 4.1. Rock Magnetic Homogeneity

[19] Three important factors to be considered when assessing rock magnetic homogeneity are the mineralogy, the magnetic grain size, and the magnetic concentration.

<sup>1</sup>Auxiliary materials are available in the HTML. doi:10.1029/2006JB004477.

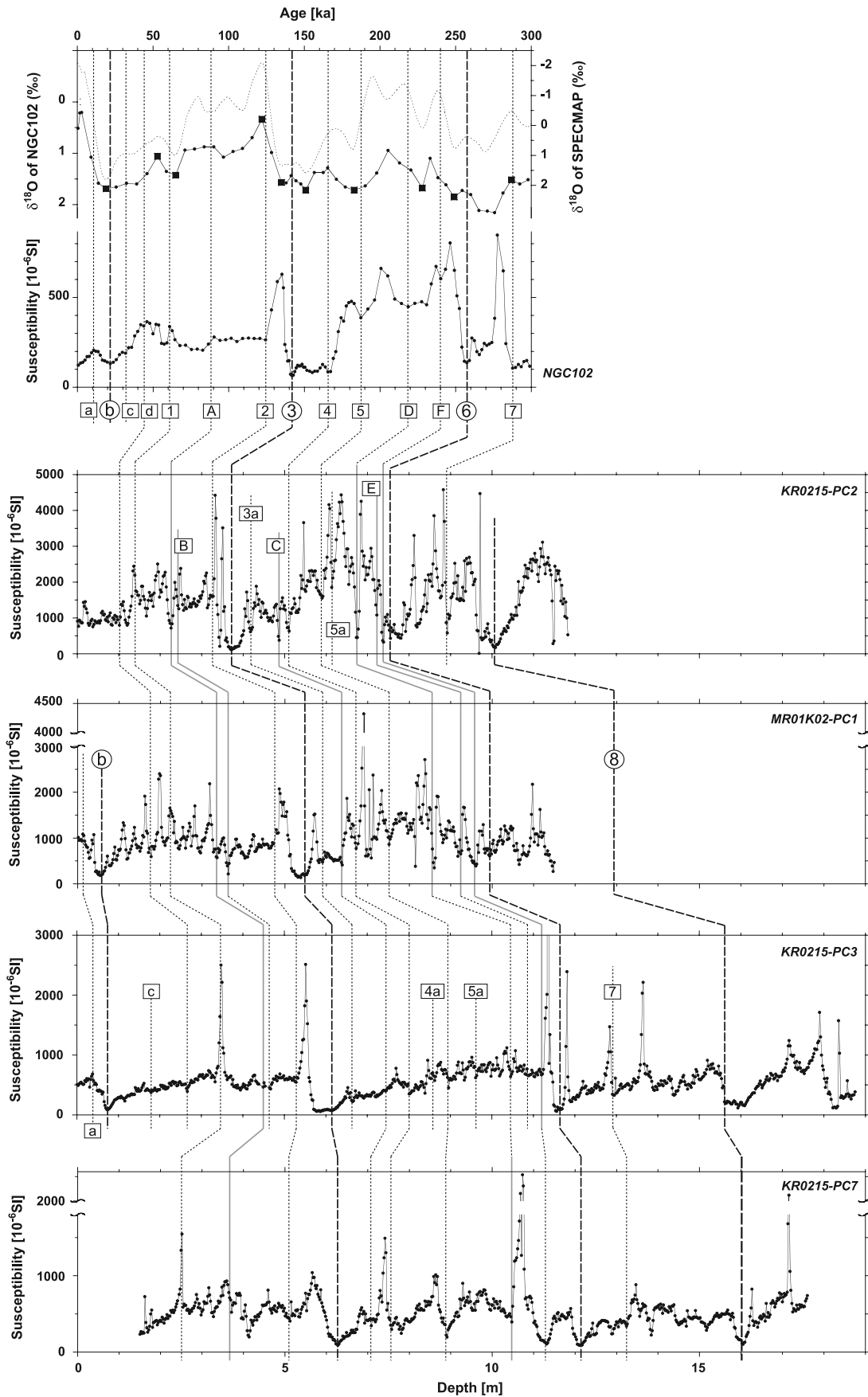


Figure 2

[20] The present cores show large decreases of the S-ratios reaching as low as  $\sim 0.90$  at several horizons (Figures 5 and 6). These events appear to have occurred mainly at glacial periods, if the tie points and the oxygen isotope records of NGC102 [Kawahata *et al.*, 1999] are considered. Figure 7 shows obvious correlation between the S-ratio, a ratio of ARM to SIRM, and SIRM in the core KR0215-PC3: horizons with  $S_{-0.3T} < 0.95$  accompany small values of ARM/SIRM and SIRM (light gray shading surrounded by dashed line in Figure 7). This indicates that concentration of magnetic particles is low in these horizons.

[21] These horizons ( $S_{-0.3T} < 0.95$ ) display positive linear relationships between SIRMs and ratios of ARM to SIRM (open circles in Figure 8a). They give different trends from data of the horizons with  $S_{-0.3T} \geq 0.95$  in SIRM-ARM diagrams (Figures 8b and 8c). Because the ratio of ARM to SIRM is generally in inverse proportion to relative magnetic grain size [e.g., Evans and Heller, 2003], the size is considered to be large in these horizons. These prominent changes probably originate from reductive dissolution of magnetite particles, as the northwest Pacific Ocean is one of the most productive oceans [Berger, 1989]. Owing to the reduction diagenesis, fine magnetite particles may have dissolved in these horizons, and high coercivity minerals like hematite would be more resistive and survived [e.g., Karlin and Levi, 1983; Yamazaki *et al.*, 2003; Emiroglu *et al.*, 2004; Garming *et al.*, 2005; Dillon and Bleil, 2006]. This can cause a decrease in S-ratio and susceptibility and an increase in relative magnetic grain size. Similar dissolution events are recognized in all other cores (see auxiliary material), though baselines of the S-ratios slightly differ among cores (0.95 or 0.96). We exclude the remanence data at horizons showing  $S_{-0.3T} < 0.95$  or 0.96 for relative paleointensity estimation.

[22] As mentioned in the section 2, the present cores were intercalated by frequent volcanic ash layers. We should omit the remanence data at such horizons for relative paleointensity estimation. One way to distinguish these horizons is to set a quantitative criterion based on a rock magnetic parameter. Horizons giving anomalously high values of SIRM are probably associated with volcanic ash layers, though some ash layers may contain little magnetic minerals resulting in smaller SIRM. We rejected SIRMs larger than  $+1\sigma$  (standard deviation) from an average in each core ( $SIRM > SIRM_{\text{mean}} + \sigma_{SIRM}$ ). If the present SIRM data were assumed to obey the normal distribution, a probability density of the outliers was 16%. Figure 7 shows an example of the discrimination in the core KR0215-PC3. In this core, SIRMs resulted in an average and a standard deviation of 12.6 and 12.5 A/m, respectively. Horizons with SIRM  $> 25.1$  A/m were regarded as outliers. Most of these horizons accompanied sharp decreases in the ratios of ARM to

SIRM (dark gray shading in the Figure 7). In the SIRM-ARM diagram (Figure 8b), data points of these horizons (open squares) also give different trends from those of  $S_{-0.3T} \geq 0.95$  horizons (closed circles). Similar discriminations based on SIRMs were applied to all other cores (see auxiliary material).

#### 4.2. Relative Paleointensity of Each Core

[23] The intensities of NRM after AF demagnetization at 30 mT were normalized by both ARM and SIRM after the same AF levels ( $(NRM/ARM)_{30mT}$  and  $(NRM/IRM)_{30mT}$ ). These normalized intensities are presented in Figures 9 and 10 except for the nonhomogeneous horizons ( $S_{-0.3T} < 0.95$  or 0.96, or  $SIRM > SIRM_{\text{mean}} + \sigma_{SIRM}$ ). For cores NGC106 and NGC109,  $(NRM/ARM)_{15mT}$  and  $NRM_{15mT}/IRM_{20mT}$  (NRM after 15 mT demagnetization normalized by SIRM after 20 mT demagnetization) are displayed as the normalized intensities. This is because ARMs were measured only for every other sample by the blanket AF demagnetization of 15 mT, and measurement intervals of  $NRM_{15mT}/IRM_{20mT}$  were  $\sim 2.5$  cm while those of  $(NRM/IRM)_{30mT}$  were  $\sim 5$  cm. Although the intensities of  $NRM_{15mT}/IRM_{20mT}$  were derived from different coercivity intervals between NRM and the normalizer (IRM), we think they can serve as normalized intensities since they are almost linearly correlated with those of  $(NRM/IRM)_{30mT}$  for the same horizons (Figure 11).

[24] If the tie points are considered, all nine records show similar variations. The intercore consistency suggests that reliable relative paleointensity records were obtained from the sediments. However, the ARM and IRM normalizations do not agree exactly with each other (dotted and solid lines in Figures 9 and 10). We prefer IRM to ARM as the normalizer for the present relative paleointensity estimations because acquisitions of ARMs are considered to be significantly influenced by magnetic interactions among magnetic grains in the northwest Pacific siliceous sediments [Yamazaki, 1999]. Acquisition of SIRM is also thought to be affected by the interactions, but it seems less sensitive than that of ARM. Although an effect of the magnetic interaction on DRM acquisition has not yet been understood well, normalizations by ARM might overcompensate magnetic concentration changes if the interaction on DRM was less sensitive than ARM but comparable to IRM.

[25] Except for the horizons affected by magnetite dissolution ( $S_{-0.3T} < 0.95$  or 0.96), there is an inverse correlation between SIRMs and ratios of ARM to SIRM in the present sediments (e.g., closed circles and open squares in Figure 8a). These relations are similar to the observation in the work of Yamazaki [1999]. Sugiura [1979] experimentally showed that the ratios of ARM to SIRM are in inverse proportion to logarithm of the concentration of magnetites. He concluded that ARM acquisition is sensitive

**Figure 2.** Magnetic susceptibilities of the piston cores. They show similar peaks and troughs among the records so that they can be tied based on the susceptibilities. The oxygen isotope records of NGC102 (closed symbols, top panel [Kawahata *et al.*, 1999]) and SPECMAP (dotted line, top panel [Imbrie *et al.*, 1989; McIntyre *et al.*, 1989]), and the susceptibility curve of NGC102 (second panel from the top) are shown for comparison. Closed squares in the top panel are control points in the work of Kawahata *et al.* [1999]. The tie points are indicated by numbers, alphabets, or their combinations. Dashed and dotted lines show prominent troughs and several characteristic troughs and peaks between the prominent troughs, respectively (see text). These depths are summarized in Table 2. The identified volcanic ash layers in the work of Suganuma *et al.* [2006] (boldface, Table 2) are displayed as gray lines.

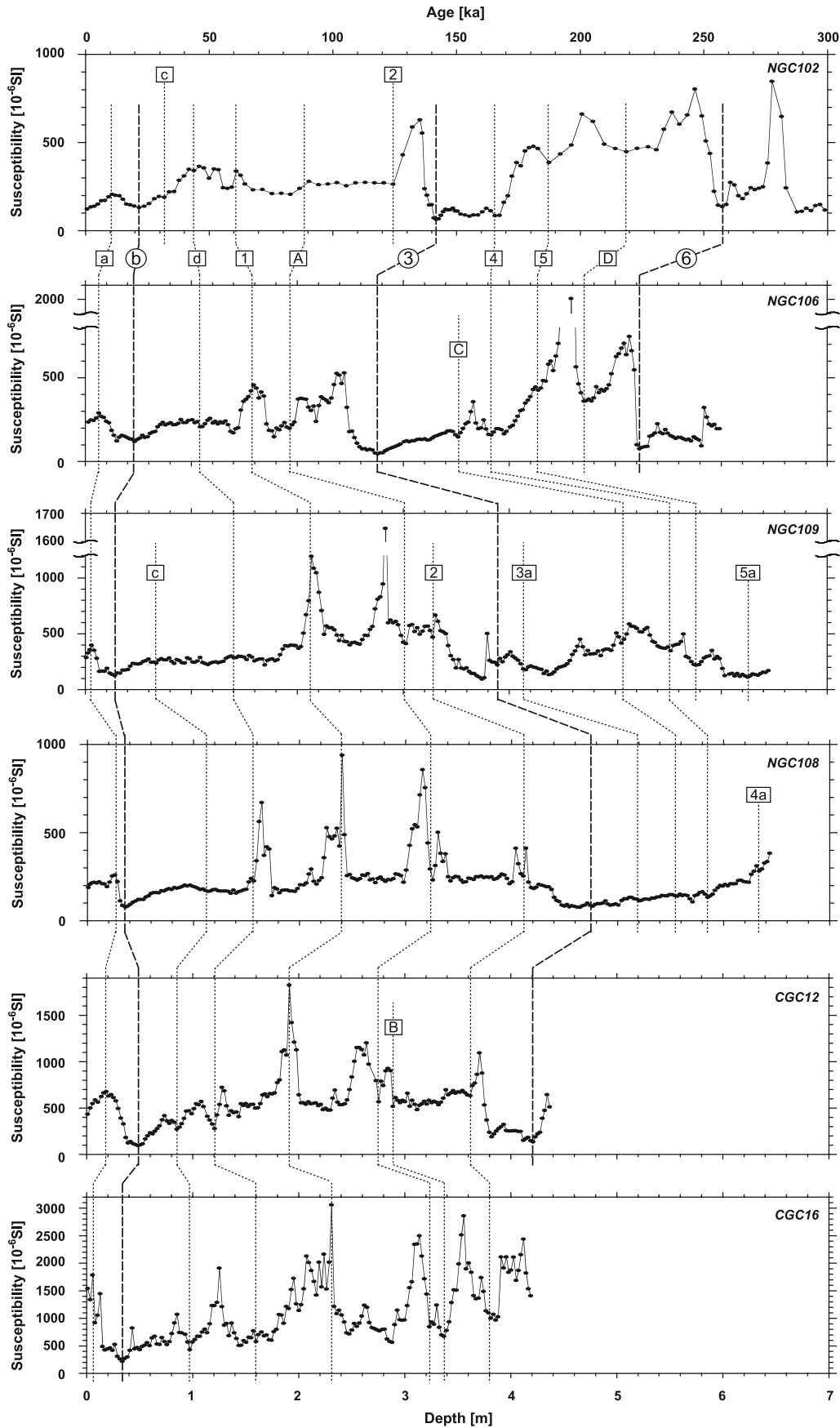
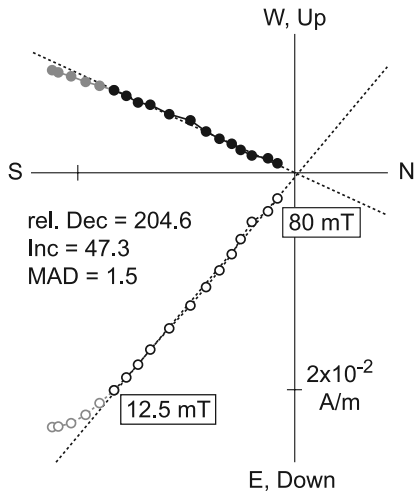


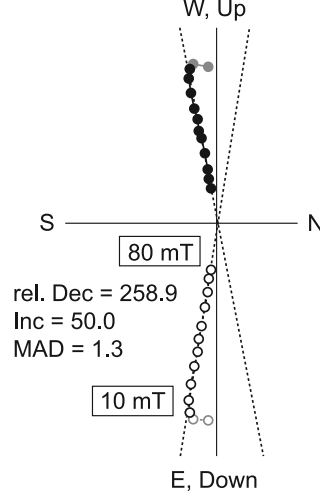
**Figure 3.** Magnetic susceptibilities of the gravity cores. The tie points are indicated by numbers, alphabets, or their combinations. These depths are summarized in Table 2.

(A)

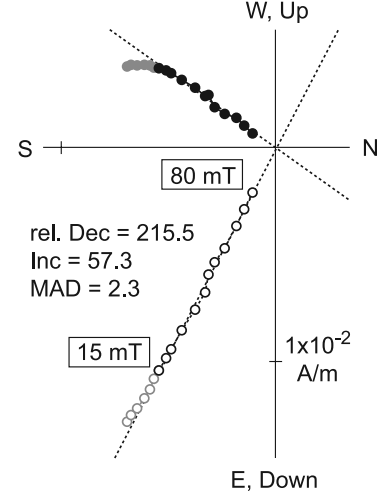
NGC106, 2.01 m



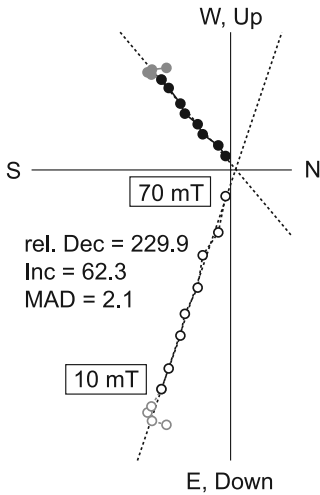
NGC108, 0.04 m



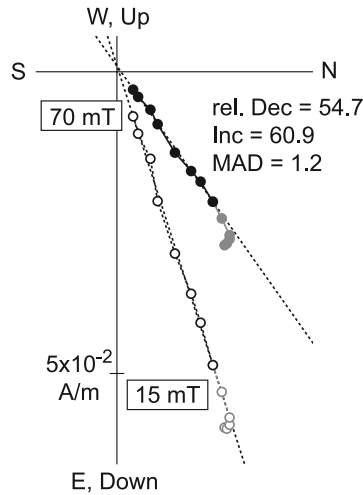
NGC109, 0.45 m



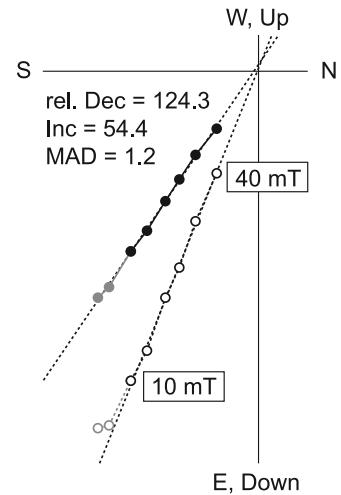
KR0215-PC2, 4.67 m



KR0215-PC3, 3.15 m

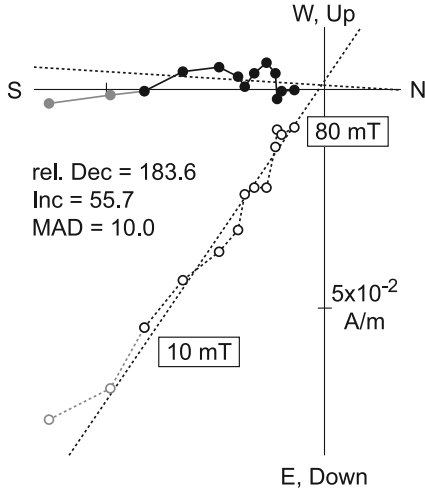


MR01K02-PC1, 10.15 m



(B)

CGC16, 0.27 m



KR0215-PC3, 5.94 m

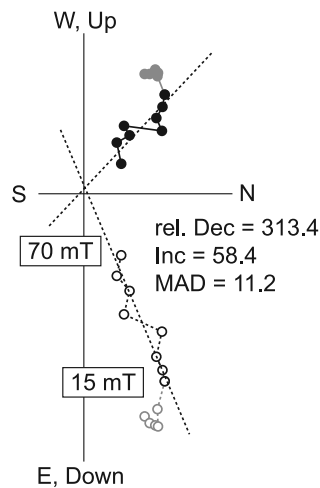


Figure 4

to magnetic interaction: stronger magnetic interaction reduces acquisition efficiency of ARM. Since SIRM is considered to represent concentration of magnetic minerals, stronger magnetic interactions result in smaller ARM/SIRM ratios, which would be responsible for the inverse correlation as shown in Figure 8a. Although the ratio of ARM to SIRM is often used as a magnetic grain-size proxy, this may not be valid for the sediments with large variation in magnetic concentration [Yamazaki and Ioka, 1997]. Variations in ARM/SIRM of the present sediments do not necessarily reflect changes in magnetic grain size. If the ratio of ARM to SIRM reflected changes in the grain size, Figure 8a suggested that the grain size was smaller in the glacial periods (large ARM/SIRM) as SIRMs of the present sediments are small in these periods. There is no such sedimentological evidence in the northwest Pacific [e.g., Rea, 1994].

[26] For the horizons affected by reduction diagenesis, there are positive linear relationships between SIRMs and ratios of ARM to SIRM (open circles in Figure 8a). The grain size effect is considered to dominate the effect of magnetic interaction.

### 4.3. Stacked Paleointensity Record

[27] As mentioned in the previous subsection, we adopted IRM as the present normalizer. From the relative paleointensity proxies of the nine cores ((NRM/IRM)<sub>30mT</sub> or NRM<sub>15mT</sub>/IRM<sub>20mT</sub>; Figures 9 and 10), a stacked record is constructed by the following procedure.

[28] 1. The depth of each core was converted into a common scale by linear interpolations between the tie points. We selected KR0215-PC3 as a reference core because its length is the longest among the present cores (Table 1) and its site is at the center of the study area (Figure 1). The relative paleointensity proxy of the nine cores is presented in Figure 12 against the common scale (depth of KR0215-PC3). It can be recognized that all curves show very consistent variations.

[29] 2. The conversions in (1) resulted in variable data intervals. Because data intervals should be basically the same for a construction of a stacked record, we resampled each record by a common interval of 1 cm with linear interpolations. After the resampling, average of the relative paleointensity proxy of each core was adjusted to unity.

[30] 3. In each record, a few paleointensity proxy data showed very large deviation from the unity. We discarded such data at this stage since they are considered as outliers. A threshold is set to be triple standard deviations ( $\pm 3\sigma$ ). Assuming the normal distribution, an out-of-range probability corresponds to 0.3%. For example, the record of KR0215-PC3 gave a standard deviation of 0.374 (1541 data points). Seven data points at 6.82–6.83 m, 10.95–10.96 m, and 11.02–11.04 m resulted in relative paleointensities more than 2.12. We discarded these data.

[31] 4. The remaining data were finally merged into a stacked record. This was done by calculating an average and

a standard error ( $\sigma_E$ ) for each resampled depth if number of data points are not less than three ( $N \geq 3$ ).

[32] Among the cores, age models based on the oxygen isotope stratigraphy were obtained for two cores, NGC102 (last 300 kyr [Kawahata *et al.*, 1999]) and NGC108 (last 180 kyr [Maeda *et al.*, 2002]). We incorporate these models into the stacked record, using the tie points (Table 2). If the model of NGC102 is adopted, the stacked record represents relative paleointensity variations in the northwest Pacific for the last 250 kyr (NOPAPIS-250, Figure 13). Although this age model offers a timescale of the last 300 kyr, the present stack lacks in the periods of around 20–25 ka, 135–145 ka, 205–210 ka, and 240–300 ka. This is mainly because S-ratios of the present cores decreased as low as  $\sim 0.90$  in these horizons or SIRMs were large, suggesting the volcanic ash layers for these horizons (section 4.1). When converting depths to ages, the horizons of the Aso-4 and Ata-Th volcanic ash layers (444 and 1125 cm depth of KR0215-PC3: the tie points of “A” and “F”) were adjusted to their documented ages of 88 and 240 ka, respectively [Oba, 1991; Machida and Arai, 2003].

## 5. Discussion

### 5.1. Difference Between the IRM and ARM Normalizations

[33] We have obtained the stacked relative paleointensity record from the northwest Pacific (NOPAPIS-250, Figure 13). Although the normalized intensities by IRM were adopted for the construction of this record, it is important to examine a possible difference between IRM and ARM normalizations. Following the same procedure as described in section 4.3, an alternative stack is constructed from the ARM-normalized intensity ((NRM/ARM)<sub>30mT</sub>) of each core. In this stacking, data from NGC106 and NGC109 ((NRM/ARM)<sub>15mT</sub>) were not incorporated because measurement intervals of these data were  $\sim 5$  cm, twice as large as those of other cores. The ARM-based stack (ARM stack) is displayed in Figure 14 together with the NOPAPIS-250 curve based on the IRM normalizations (IRM stack). The number of cores stacked differ between the two records (top), but variation patterns appear to be almost the same (bottom).

[34] However, if we compare the two stacks at the same horizons, data points do not agree exactly (Figure 15a). Differences between the two stacks are up to  $\sim 50\%$ . Although a correlation coefficient in Figure 15a resulted in a high value of 0.925, *t*-test for correlated data gives a *t* value of  $-2.87$ , which corresponds to a probability of 0.419%. The *t*-test statistically examines whether or not the means of two populations (different standard deviations) are different. The present result indicates that the two stacks are statistically distinguishable from each other at the 99.6% level. One may think that this discordance probably originates from the difference in the number of core stacked (Figure 14, top), but it does not seem to be true since the

**Figure 4.** Typical AF demagnetization results projected onto orthogonal diagrams. Closed and open circles denote horizontal and vertical components, respectively. Almost all samples showed single stable components after removals of secondary remanences at 10–20 mT. (a) About 90% of the samples yielded  $MAD < 5^\circ$ . (b) Rest 10% of the samples showed more noisy demagnetization behavior.

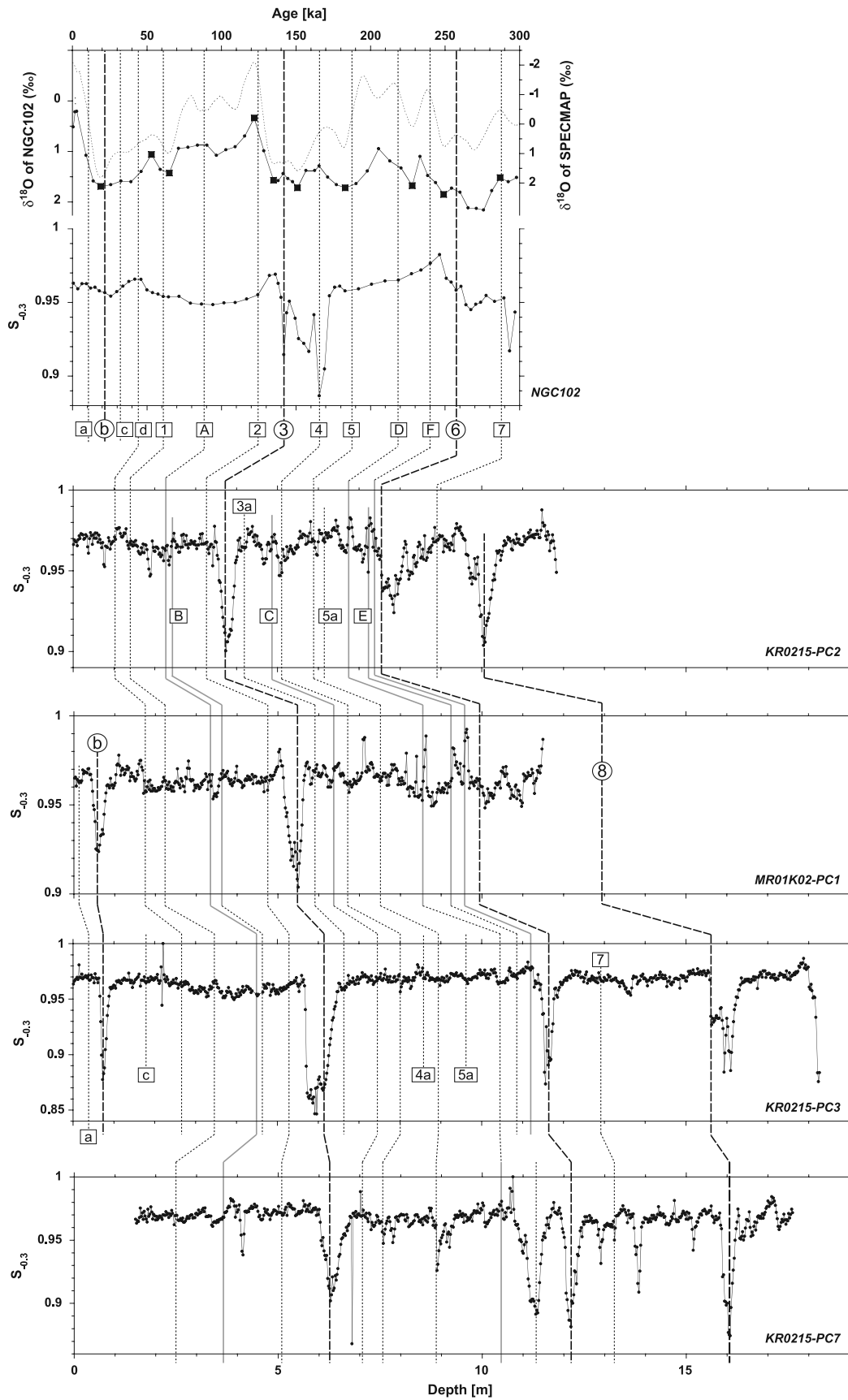


**Figure 5.** S-ratios ( $S_{-0.3T}$ ) of the piston cores. The tie lines are referred from Figure 2. The oxygen isotope records of NGC102 (closed symbols [Kawahata *et al.*, 1999]) and SPECMAP (dotted line [Imbrie *et al.*, 1989; McIntyre *et al.*, 1989]), and the S-ratio of NGC102 are shown for comparison.

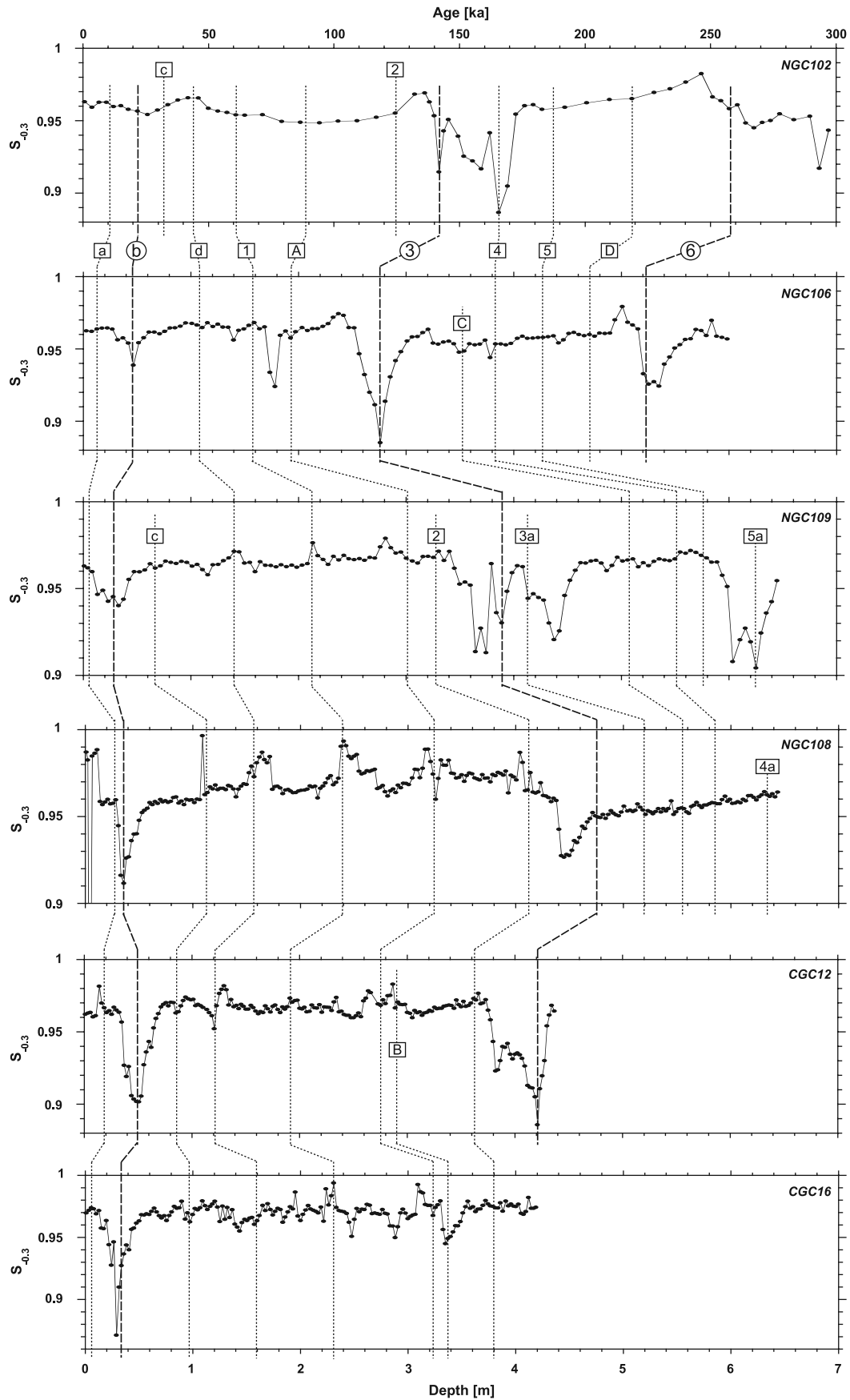


**Figure 6.** S-ratios ( $S_{-0.3T}$ ) of the gravity cores. The tie lines are referred from Figure 3. For the S-ratio of NGC102, data are illustrated against the age model by Kawahata *et al.* [1999].

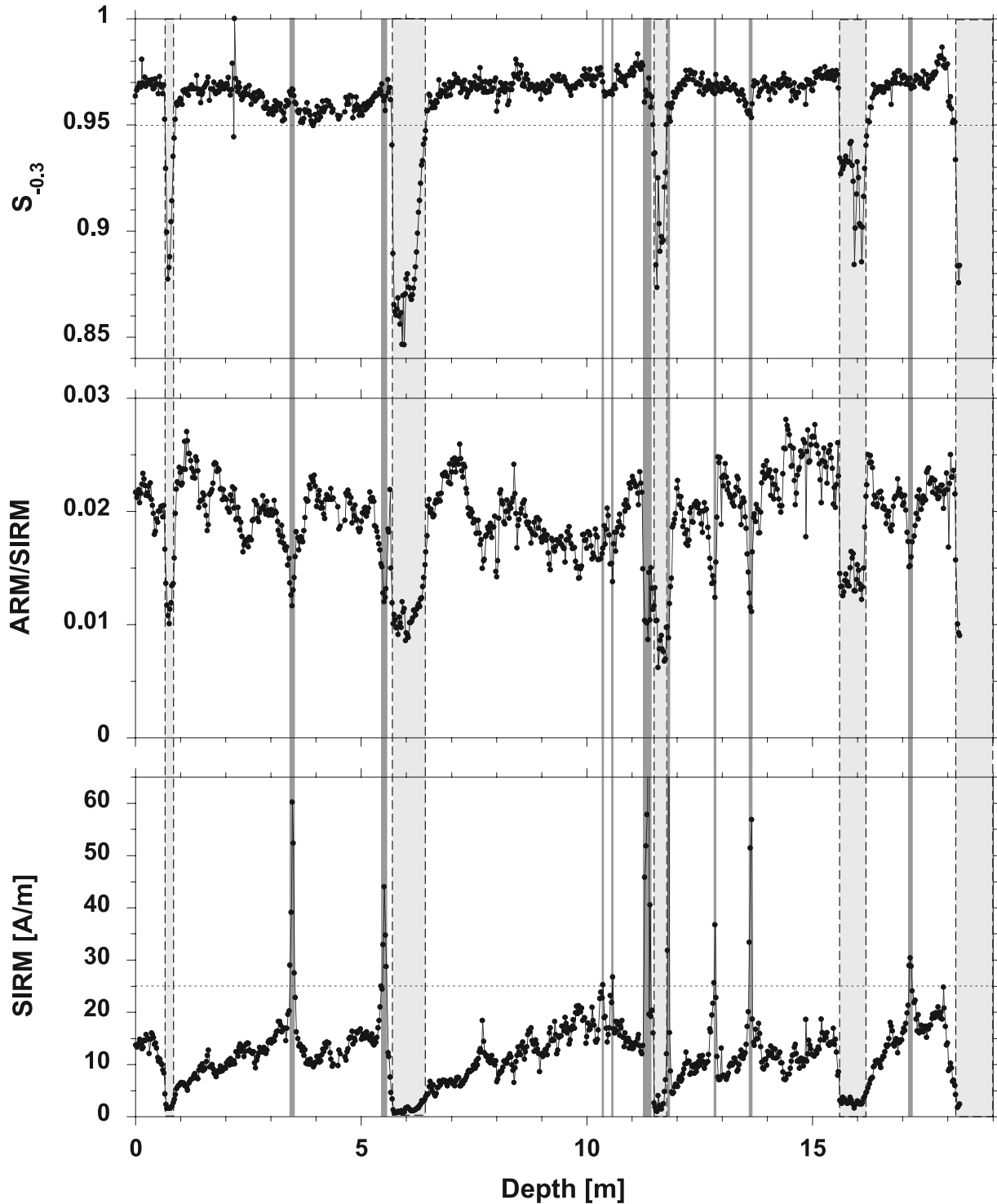


**Figure 7.** Down-core variations of the S-ratio ( $S_{-0.3T}$ , top panel), the ratio of ARM to SIRM (middle), and the SIRM (bottom) in the core KR0215-PC3. It is obvious that the horizons with  $S_{-0.3T} < 0.95$  accompany small values of ARM/SIRM and SIRM (light gray shading surrounded by dashed line). Also, the layers showing anomalously high SIRMs ( $SIRM > SIRM_{\text{mean}} + \sigma_{SIRM}$ ; 25.1 A/m) resulted in the small ARM/SIRM (dark gray). Remanence data from these horizons are excluded from the relative paleointensity estimation.

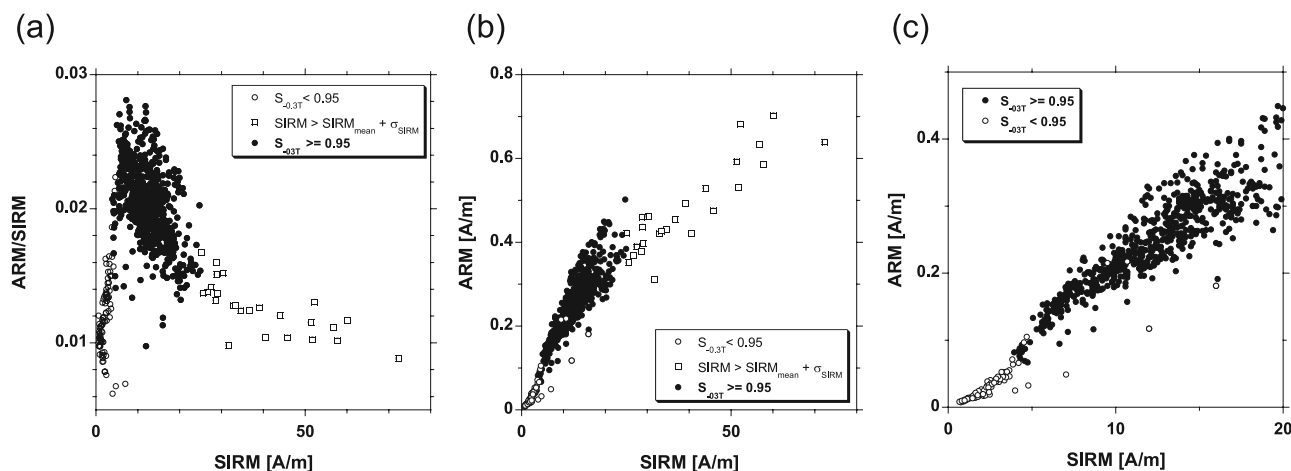


**Figure 8.** ARM and SIRM data from the core KR0215-PC3. SIRM is displayed against (a) ratio of ARM to SIRM, (b) ARM, and (c) its closeup. Open circles, open squares, and closed circles indicate data from the horizons with  $S_{-0.3T} < 0.95$ ,  $SIRM > SIRM_{mean} + \sigma_{SIRM}$  (25.1 A/m), and  $S_{-0.3T} \geq 0.95$ , respectively.

extent of the discordance is independent of the difference in the number of core stacked (Figure 15b).

[35] An interesting feature observed in Figure 15a is that some of the data points appear to plot along a streak (slope with  $\sim 1.25$  in the lower left region of the figure). This behavior becomes clearer if the normalized intensities by ARM and IRM are compared for each core (Figure 15c). They originate from small values of the normalized intensities, which correspond to the horizons at  $\sim 200$  ka (considered to record the Iceland Basin Excursion, see next subsection). Because NRM of these horizons are very small compared to other horizons, differences in acquisition efficiencies between IRM and ARM (section 4.2) might appear pronouncedly in the normalized intensities of these horizons (less ARM acquisitions resulted in larger normalized intensities).

[36] The discordance between the IRM stack and the ARM stack also makes difference in histograms of the normalized intensities. If normal distributions are assumed (upper histograms of Figures 16a and 16b), we can directly compare statistical parameters because the averages of the two stacks were already adjusted to unity. For instance, standard deviations are 0.325 (IRM stack) and 0.317 (ARM stack). This means that variations in the intensities of SIRM are relatively smaller than those in the ARM intensities for the present sediments. The skewnesses and kurtosises are 0.0907 and 0.480 (IRM stack) and 0.184 and 0.672 (ARM stack), respectively. These parameters are generally used as a measure of the normality; if a data set is normally distributed, both parameters should be zero. The larger the skewness, the greater the asymmetry of the distribution. Also, the larger the kurtosis, the narrower the peak of the distribution. In this sense, it can be said that the histogram of the IRM stack is closer to the normal distribution than that of the ARM stack, though  $\chi^2$  tests suggest that neither stack is normally distributed (at the 99.9% level).

[37] Log-normal distributions are often quoted as alternative possible paleointensity distributions [e.g., Tanaka et al., 1995]. To consider about these distributions, data sets of

the IRM stack and the ARM stack are converted into logarithms and averages are adjusted to  $-1$ . Both histograms are shown in lower panels of Figures 16a and 16b. In contrast to the case of the normal distributions, skewnesses and kurtosises resulted in  $-1.74$  and  $5.21$  (IRM stack) and  $-1.60$  and  $4.55$  (ARM stack). This means that the histogram of the ARM stack is closer to the log-normal distribution than that of the IRM stack. However,  $\chi^2$  tests indicate that neither stacks obey to the log-normal distributions (at the 99.9% level).

[38] For comparison, we show histograms of paleointensity data from volcanic rocks (Figure 16c). They were constructed from selected virtual axial dipole moment (VADM) data from the latest absolute paleointensity database [Perrin and Schnepf, 2004]. Selection criteria are as follows, which are almost the same as those used in the previous studies treating paleointensity databases [e.g., Biggin and Thomas, 2003; Heller et al., 2002; Selkin and Tauxe, 2000]: (1) Ages range between 10 and 250 ka. (2) Paleointensities are obtained by the Thellier method with pTRM check (T+). (3) Averaged paleointensity for each cooling unit is calculated from not less than three individual determinations ( $N \geq 3$ ). (4) The standard deviation of each average is within 20% ( $\sigma \leq 20\%$ ). One hundred forty-five Thellier data passed these criteria. They give the average and standard deviation of  $7.09 \times 10^{22} \text{ Am}^2$  and  $2.61 \times 10^{22} \text{ Am}^2$ , respectively, if the normal distribution is assumed. The ratio of the standard deviation to the average is 37%, higher than that of the IRM stack and the ARM stack ( $\sim 32\%$ ).  $\chi^2$  test did not reject the hypothesis that they obey to the normal distribution at the 95.0% level. Although small values of a skewness (0.0430) and a kurtosis ( $-0.651$ ) suggest the normality for the volcanic histogram (the upper panel in Figure 16c), it might not be appropriate to calculate the statistical parameters with an assumption of the normal distribution. This is because the volcanic data appears to result in a bimodal distribution rather than the normal distribution: there are two peaks around  $5 \times 10^{22} \text{ Am}^2$  and  $9 \times 10^{22} \text{ Am}^2$  (the upper panel in Figure 16c). The situation

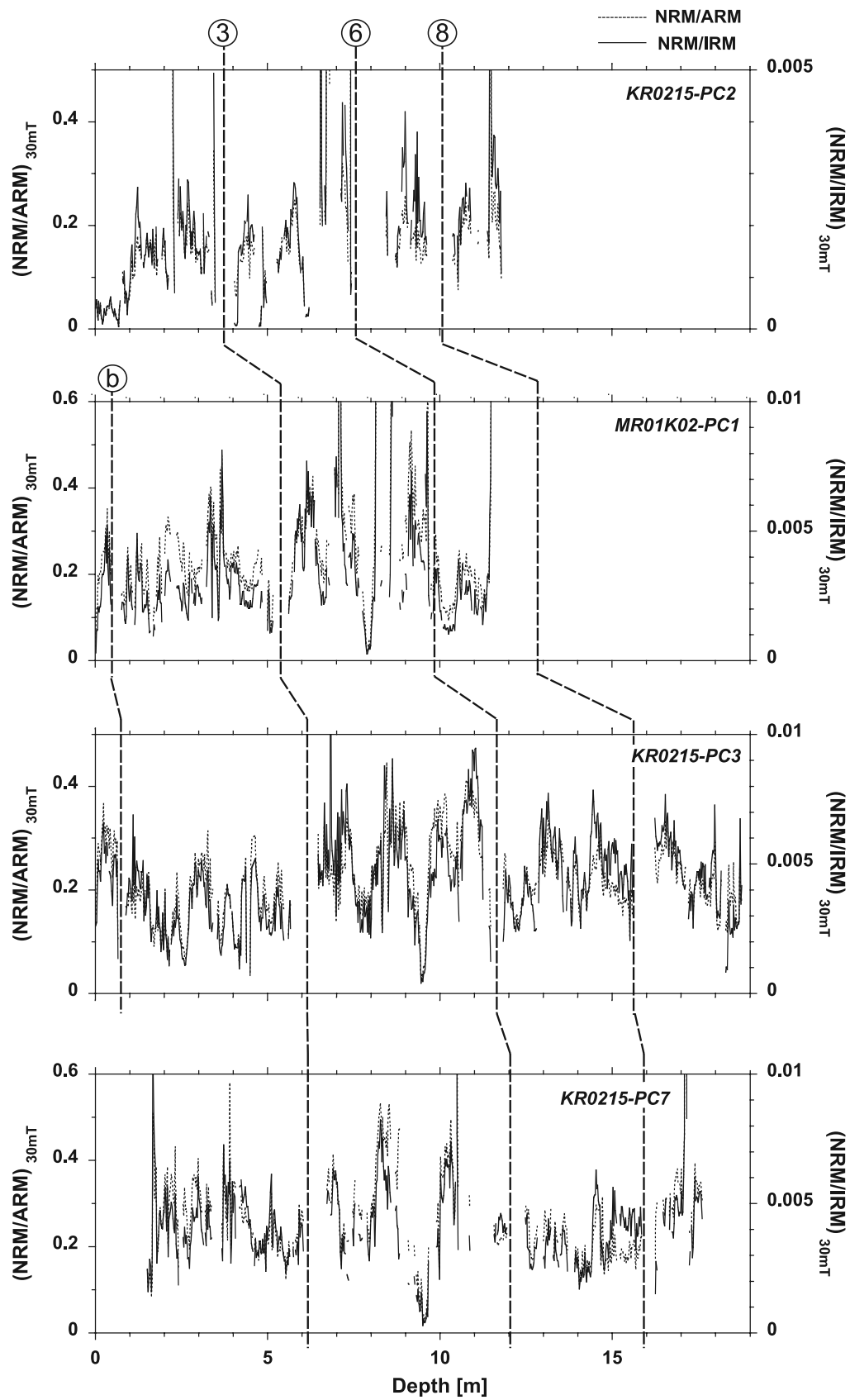


**Figure 9.** Normalized intensities of the piston cores. Dotted and solid lines indicate NRMs normalized by ARM and IRM, respectively. The major tie lines are referred from Figure 2. Data are presented except for the non-homogeneous horizons ( $S_{-0.3T} < 0.95$  or  $0.96$ , or  $SIRM > SIRM_{mean} + \sigma_{SIRM}$ ).

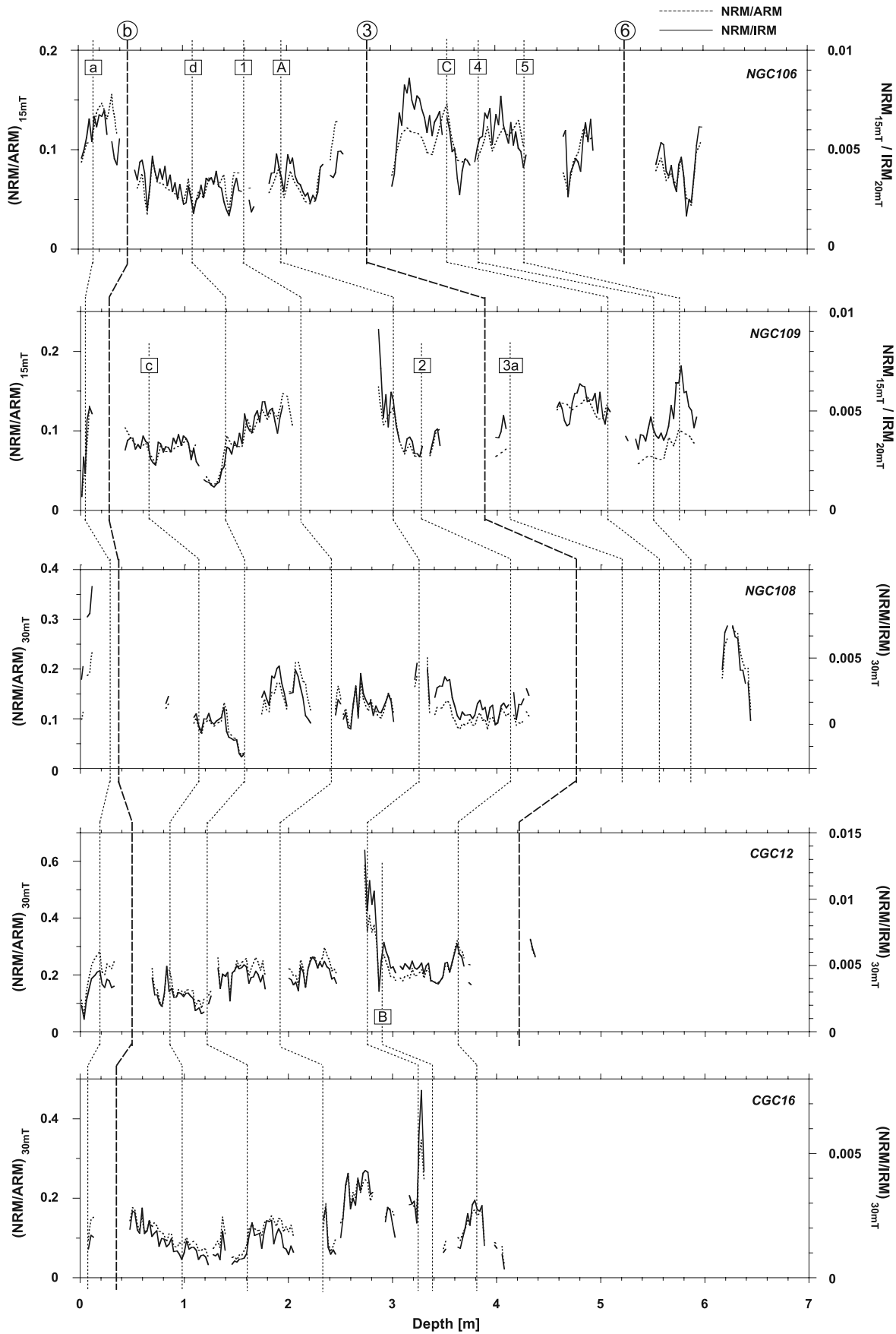
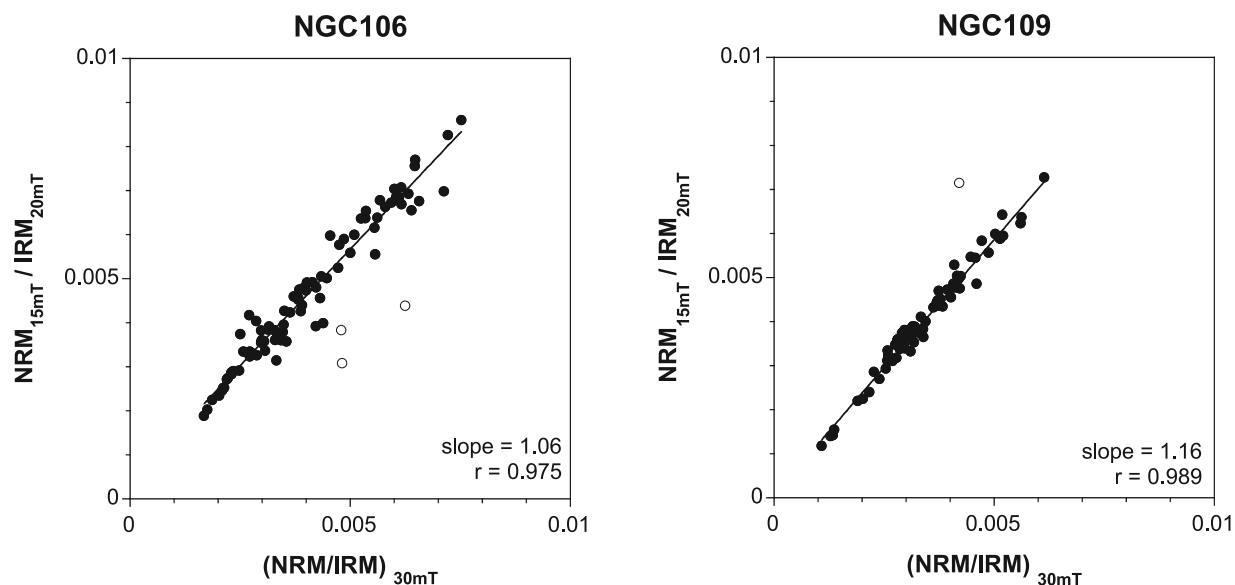


Figure 10. Normalized intensities of the gravity cores. The tie lines are referred from Figure 3.



**Figure 11.** Relations between  $(\text{NRM}/\text{IRM})_{30\text{mT}}$  and  $\text{NRM}_{15\text{mT}}/\text{IRM}_{20\text{mT}}$  for cores NGC106 and NGC109. Each data point is from the same horizon. Except for some outliers (open circles), values of  $\text{NRM}_{15\text{mT}}/\text{IRM}_{20\text{mT}}$  are almost linearly correlated with those of  $(\text{NRM}/\text{IRM})_{30\text{mT}}$  (correlation coefficients are 0.975 and 0.989 for the closed symbols).

might turn out slightly for the better if the log-normal distribution is considered (lower panel in Figure 16c). However, there is an unusual population in the bin between  $e^{2.1}$  and  $e^{2.4}$ , and  $\chi^2$  test rejects the hypothesis that they are log-normally distributed (at the 99.7% level).

[39] Since many paleomagnetists have considered the Thellier method as the most reliable absolute paleointensity technique for volcanic rocks [e.g., *Goguitchaichvili et al.*, 2004], the bimodal distribution may be true random samplings of the geomagnetic field. In this sense, neither histograms of the IRM stack nor the ARM stack are considered to reflect the geomagnetic field behavior. Recent studies, however, have revealed that the Thellier method on volcanic rocks occasionally overestimates paleointensities up to about twice as high as true values [e.g., *Yamamoto et al.*, 2003; *Yamamoto and Tsunakawa*, 2005]. One of the possible causes is acquisition of thermochemical remanent magnetization (TCRM) during formation of lavas [*Yamamoto*, 2006]. The higher peak of the bimodal distribution (around  $9 \times 10^{22} \text{ Am}^2$ ) possibly originates from a cluster of overestimated paleointensities. The normal distribution with a single peak or the log-normal distribution without the unusual population might truly reflect the geomagnetic field. At present, it is difficult to conclude whether or not a variation of the geomagnetic dipole moment obeys to the normal distribution or the log-normal distribution. However, it is interesting that the IRM stack gives the normal-distribution-like histogram whereas the ARM stack yields the log-normal-like one, though the  $\chi^2$  tests rejected the hypotheses of the both distributions.

## 5.2. Relative Paleointensity Variation During the Last 250 kyr

[40] If the NOPAPIS-250 curve reflects the dipolar nature of the geomagnetic field, it should show variations similar

to relative paleointensity records from other regions. There are several high-resolution paleointensity records reported from the north Atlantic. The Portuguese stack was constructed from six sediment cores by *Thouveny et al.* [2004]. The Azores stack was compiled by *Lehman et al.* [1996] based on results from three sediment cores. The records of ODP Site 983 and 984 were reported by *Channel* [1999]. In the western equatorial Pacific, *Yamazaki and Oda* [2004, 2005] studied the core MD982183.

[41] All these records, including the global paleointensity stack of the last 800 kyr (Sint-800 [*Guyodo and Valet*, 1999]), generally show similar variation patterns in relative paleointensities (Figure 17). Many paleointensity lows are recognized in common (dashed lines of A-I in Figure 17). The ages of the lows slightly differ among the records, but it probably originates from an uncertainty in the age model of each record. For instance, the low indicated by “H” occurs at  $\sim 200$  ka in the NOPAPIS-250 curve,  $\sim 195$  ka in the record of MD982183, and  $\sim 185$ – $190$  ka in other records. The difference observed in the NOPAPIS-250 curve could be attributed to a lack of age control points between 183 ka and 228 ka in the oxygen isotope record of NGC102 (squares in Figure 2). Therefore it appears that the NOPAPIS-250 curve mainly represents the global dipole signal. The observed paleointensity lows occurred simultaneously on the globe. Note that two of the lows are not so clear in the Sint-800 (B and D in Figure 17). Even for the other lows in the Sint-800, troughs are not so low compared with other records. This is because the Sint-800 is a compilation of 33 relative palaeointensity records from the globe. Stacking of many records probably suppressed the amplitude of the resultant curve, though records of two cores from the Azores stack (SU92-18 and SU92-19) and those of ODP Site 983 and 984 were integrated into the Sint-800. The

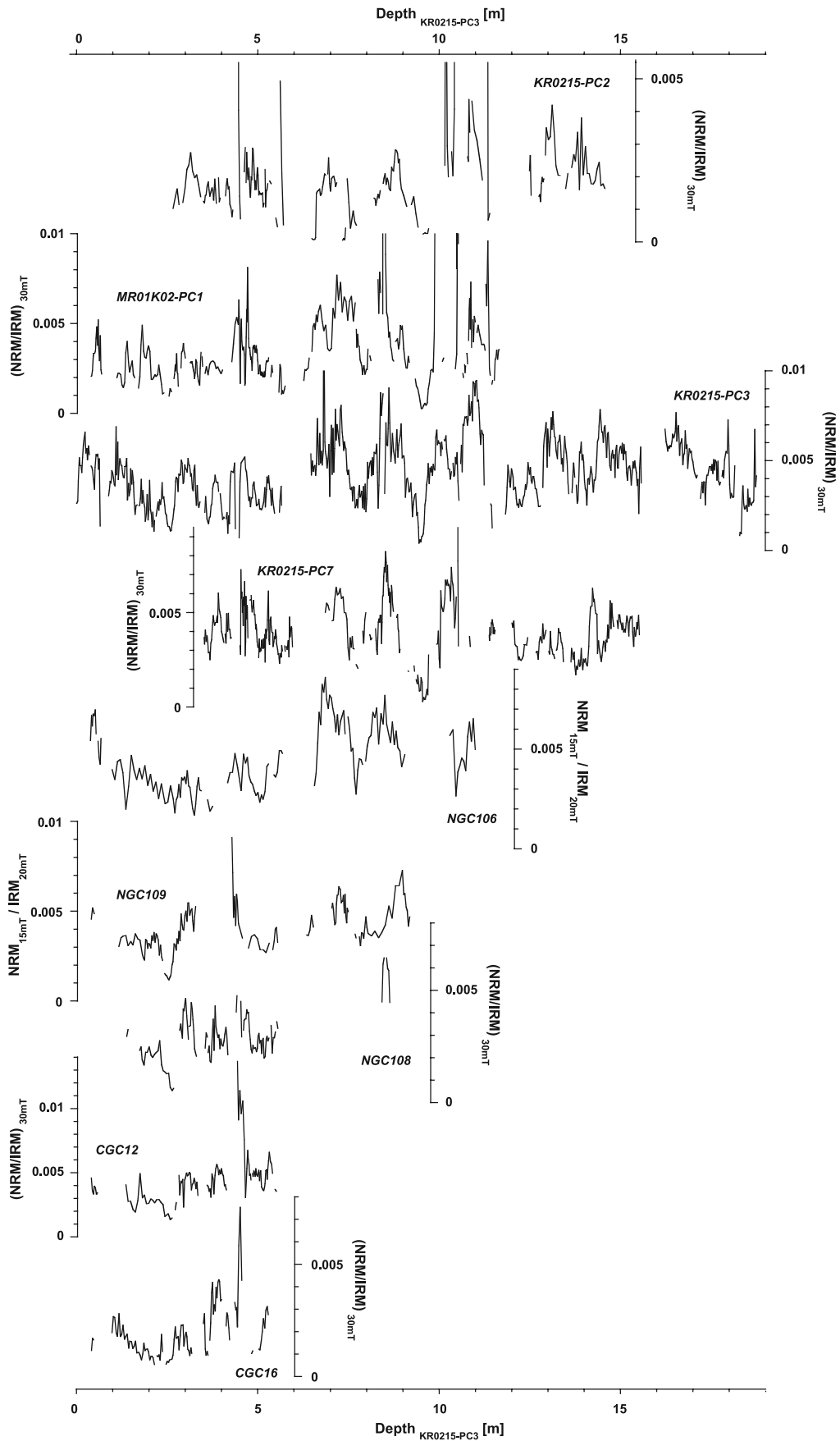


**Figure 12.** All relative paleointensity proxies ((NRM/IRM)<sub>30mT</sub> or NRM<sub>15mT</sub>/IRM<sub>20mT</sub>) against the common depth scale (depth of KR0215-PC3).

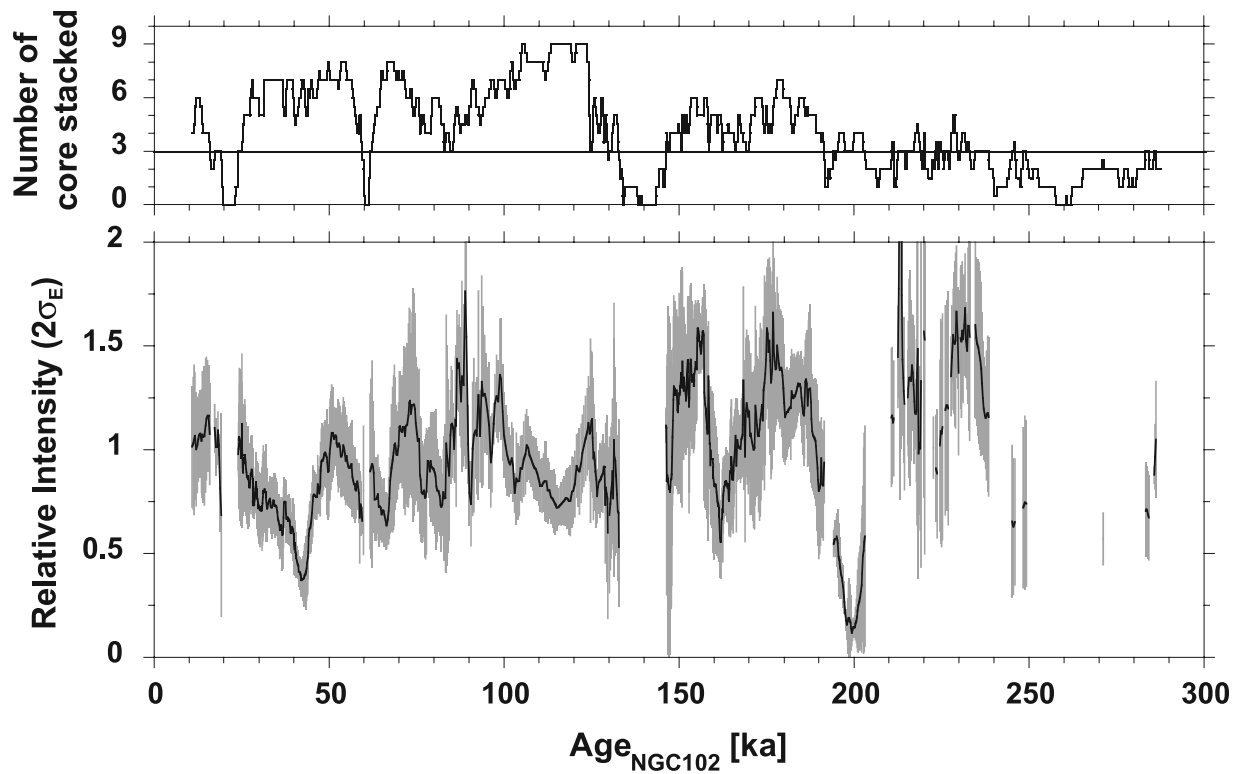


**Figure 13.** Northwest Pacific paleointensity stack NOPAPIS-250. Upper and lower panel represents number of core stacked and relative paleointensity, respectively. In the lower panel, the average (bold) and double standard error ( $2\sigma_E$ , gray) are indicated.

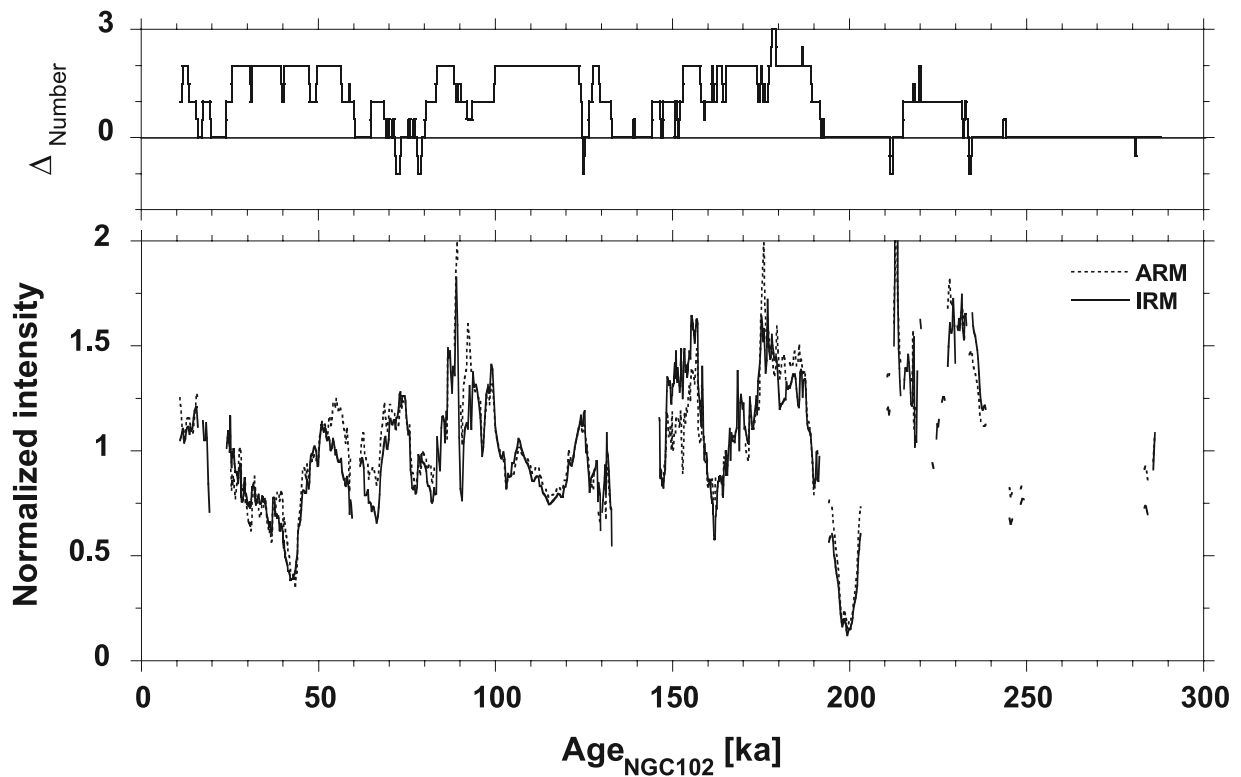


**Figure 14.** Comparison of the ARM stack (dashed line) and the IRM stack (solid line). Note that data from NGC106 and NGC109 were not incorporated into the former stack. Differences in the number of core stacked ( $\Delta_{\text{Number}}$ ) between the two stacks are indicated in the top panel.

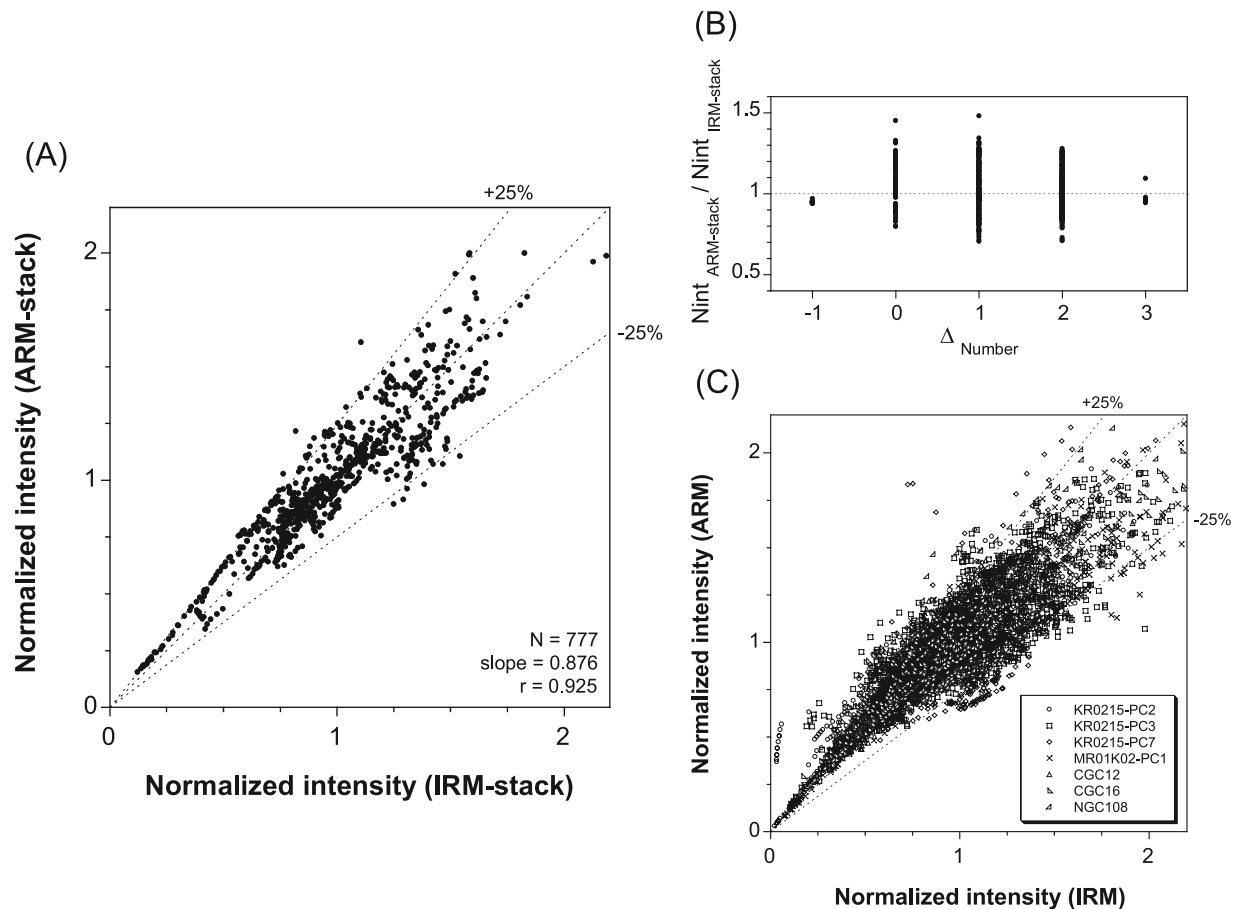


**Figure 15.** (a) Comparison of the normalized intensities between the ARM stack and the IRM stack at the same horizons. Data points do not agree exactly. (b) Relations between the difference in the number of core stacked ( $\Delta_{\text{Number}}$ ) and ratio of the normalized intensities (ARM normalized intensities ( $Nint_{\text{ARM stack}}$ ) to IRM normalized intensities ( $Nint_{\text{IRM stack}}$ ). The ratios are independent of  $\Delta_{\text{Number}}$ . (c) Comparison of the normalized intensities by ARM and IRM in each core.

Sint-800 includes records with low sedimentation rate, so that a resolution in time does not seem to be high.

[42] Similar to other high-resolution records [e.g., *Thouveny et al.*, 2004], the ages of the recognized paleointensity lows (A-I in Figure 17) seem to correspond to reported geomagnetic excursions. According to *Oda* [2005], who extensively compiled excursion records from literature, probably more than 18, possibly up to 23 excursions may have occurred in the Brunhes Chron, and most of them are associated with relative paleointensity lows. The bottom panel in Figure 17 is a geomagnetic timescale showing compiled timing of the possible geomagnetic excursions [*Oda*, 2005]. Fourteen possible excursions are illustrated in this timescale, 10 of which are judged to be reliably determined (labeled by names): the Hilina Pali at 18–23 ka, the Mono Lake at 32–34 ka, the Laschamp at 39–40 ka, the Norwegian-Greenland Sea at 60–80 ka, the Blake at 115–122 ka, the Albuquerque at 140–160 ka, the Iceland Basin at 180–190 ka, the Jamaica/Pringle Falls at 210–220 ka, the Fram Strait at 255–265 ka, and the Kolbeinsey Ridge at 280–290 ka [*Oda*, 2005]. Six out of the nine lows recognized in the NOPAPIS-250 curve can be correlated with these excursions: A for the Laschamp, C for the Norwegian-Greenland Sea, F for the Blake, G for the

Albuquerque, H for the Iceland Basin, and I for the Jamaica/Pringle Falls. The ages of these correlated lows generally agree with those of compilations by *Oda* [2005], though some offsets in age are observed. Maximum of the differences are  $\sim 15$  kyr. Because the North Atlantic sediments usually accompany the oxygen isotope stratigraphy and the resolution of the ages are generally higher than that of our cores in the northwest Pacific based on tephro-stratigraphy, the differences may happen. In fact, the calibration points of the present age model are at 19, 53, 65, 122, 135, 151, 183, 228, 249, and 287 ka in the oxygen isotope record of NGC102 (squares in Figure 2), and 88 and 240 ka in the tephro-stratigraphy (Aso-4 and Ata-Th volcanic ash layers). There may be ambiguity in age up to  $\sim 15$  kyr between the ages of the correlated lows.

[43] Real paleomagnetic field changes in the northwest Pacific probably accompany larger-amplitude and higher-frequency paleointensity lows and highs than the field represented by the NOPAPIS-250 curve. Although stacking is helpful for extracting common signal from random noise, it loses a certain amount of information compared with the best quality records. KR0215-PC3 is the longest record temporally and has the highest resolution among the studied cores. The relative paleointensity proxy of KR0215-PC3

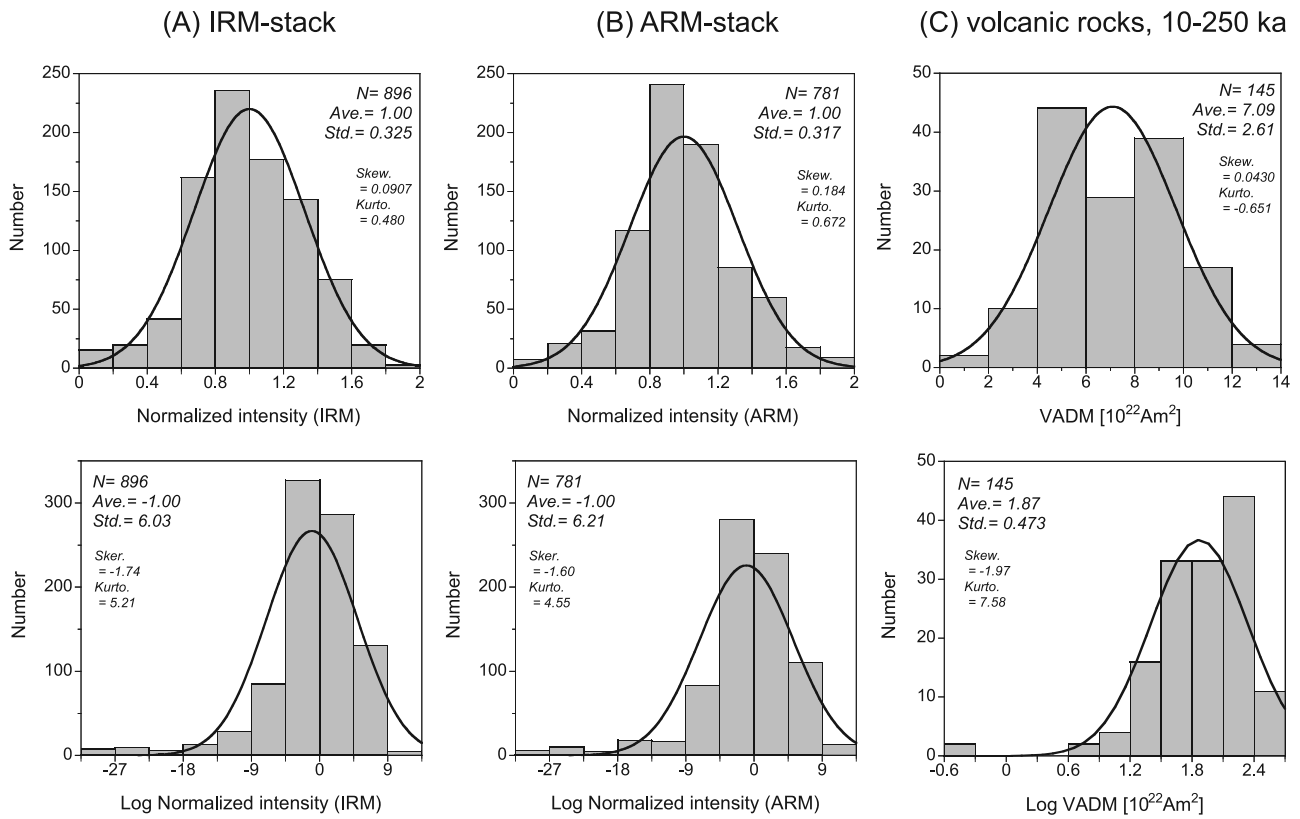


**Figure 16.** (top) Histograms of the normalized intensities and (bottom) their logarithms for (a) the IRM stack and (b) the ARM stack. (c) For comparison, similar histograms are also shown for the selected VADM data from the latest absolute paleointensity database. Solid curves are normal distribution functions computed from the averages and standard deviations of the corresponding data sets.

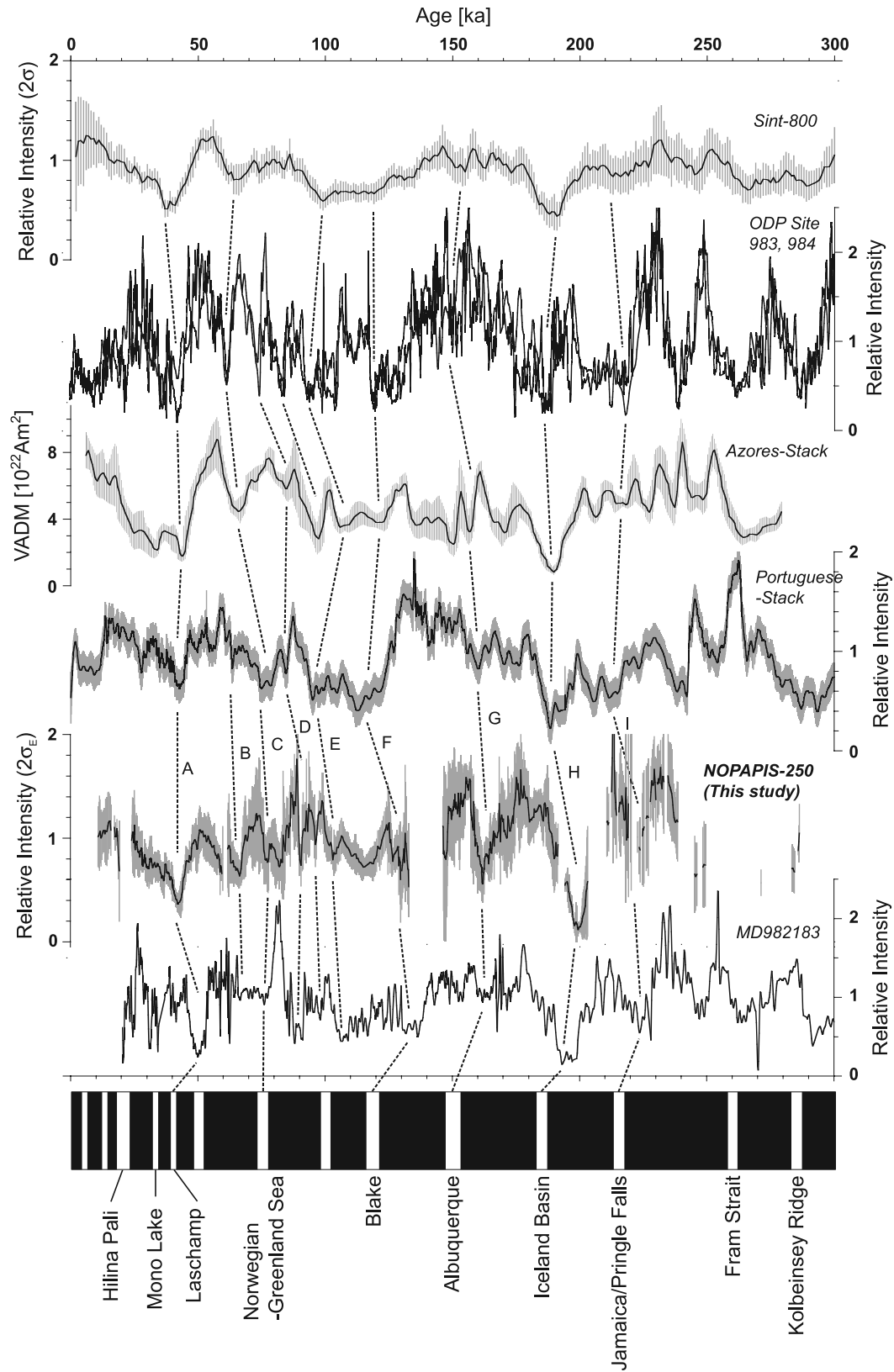


**Figure 17.** Comparison of the northwest Pacific paleointensity stack NOPAPIS-250 of this study with previously published records: Sint-800 [Guyodo and Valet, 1999], ODP Site 983 and 984 [Channel, 1999], the Azores stack [Lehman et al., 1996], the Portuguese stack [Thouveny et al., 2004], and MD982183 [Yamazaki and Oda, 2004, 2005]. Undermost panel is the geomagnetic timescale showing compiled timing of the possible geomagnetic excursions [Oda, 2005]. Fourteen possible excursions are illustrated in this timescale, 10 of which are judged to be reliably determined (labeled by names).

(Figure 12) showed larger-amplitude and higher-frequency lows and highs than the NOPAPIS-250 curve. The nature persisted throughout the core. Several paleointensity lows can be recognized from horizons deeper than  $\sim 11.5$  m, which corresponds to the oldest age of the NOPAPIS-250 curve.

[44] **Acknowledgments.** We thank Etsuko Usuda and Kazue Matsuo for thorough help of the measurements, Yusuke Suganuma for discussions on the tephrostratigraphy, Hirokuni Oda for comments on the manuscript, and those who concerned the R/V *Hakurei-maru* NH95-1, *Hakurei-maru* No.2 NH99, *Kairei* KR02-15, and *Mirai* MR01-K02 cruises for taking the cores. We are also grateful to Nicolas Thouveny for his courtesy of offering Portuguese stack data. Constructive reviews by Joseph Stoner, Gary Acton, and anonymous associate editor improved this paper. Y. Yamamoto was supported by Research Fellowships of the Japan Society for the Promotion of Science for Young Scientists. This study was partly supported by the Grant-in-Aid for Scientific Research (A)(2) 16204034 of the Japan Society for the Promotion of Science.

## References

- Berger, W. H. (1989), Global maps of ocean productivity, in *Dahlem Workshop on Productivity of the Ocean: Present and Past*, edited by W. H. Berger et al., pp. 429–455, John Wiley, Hoboken, N. J.
- Biggin, A. J., and D. N. Thomas (2003), Analysis of long-term variations in the geomagnetic poloidal field intensity and evaluation of their relationship with global geodynamics, *Geophys. J. Int.*, *152*, 392–415.
- Bloemendal, J., J. W. King, F. R. Hall, and S.-J. Doh (1992), Rock magnetism of late Neogene and Pleistocene deep-sea sediments: Relationship to sediment source, diagenetic processes, and sediment lithology, *J. Geophys. Res.*, *97*, 4361–4375.
- Channel, J. E. T. (1999), Geomagnetic paleointensity and directional secular variation at Ocean Drilling Program (ODP) Site 984 (Bjorn Drift) since 500 ka: Comparisons with ODP Site 983 (Gardar Drift), *J. Geophys. Res.*, *104*, 22,937–22,951.
- Dillon, M., and U. Bleil (2006), Rock magnetic signatures in diagenetically altered sediments from the Niger deep-sea fan, *J. Geophys. Res.*, *111*, B03105, doi:10.1029/2004JB003540.
- Emiroglu, S., D. Rey, and N. Petersen (2004), Magnetic properties of sediment in the Ria de Arousa (Spain): Dissolution of iron oxides and formation of iron sulphides, *Phys. Chem. Earth*, *29*, 947–959.
- Evans, M. E., and F. Heller (2003), *Environmental Magnetism: Principles and Applications of Enviromagnetism*, 299 pp., Elsevier, New York.
- Fukuhara, T., Y. Tanaka, K. Ikehara, and A. Nishimura (2001), Marine sediments in the western Pacific taken during the NH99 cruise (in Japanese), in *Research on Sedimentation Process in the Open Ocean*, edited by Y. Tanaka, pp. 5–76, Geol. Surv. of Jpn., Natl. Inst. of Adv. Ind. Sci. and Technol., Tsukuba.
- Garming, J. F. L., U. Bleil, and N. Riedinger (2005), Alteration of magnetic mineralogy at the sulfate-methane transition: Analysis of sediments from the Argentine continental slope, *Phys. Earth Planet. Inter.*, *151*, 290–308.
- Goguitchaichvili, A., J. Urrutia-Fucugauch, L. M. Alva-Valdivia, J. Morales, J. Riisager, and P. Riisager (2004), Long-term variation of geomagnetic field strength: A cautionary note, *Eos Trans. AGU*, *85*, 209–212.
- Guyodo, Y., and J. P. Valet (1999), Global changes in intensity of the Earth's magnetic field during the past 800 kyr, *Nature*, *36*, 234–238.
- Heller, R., R. T. Merrill, and P. L. McFadden (2002), The variation of intensity of Earth's magnetic field with time, *Phys. Earth Planet. Inter.*, *131*, 237–249.
- Imbrie, J., A. McIntyre, and A. C. Mix (1989), Oceanic response to orbital forcing in the late Quaternary: Observational and experimental strategies, in *Climate and Geosciences: A Challenge for Science and Society in the 21st Century*, edited by A. Berger, S. H. Schneider, and J.-C. Duplessy, Springer, New York.
- Ioka, N., Y. Hatakeyama, K. Ikehara, Y. Tanaka, K. Nakashima, and A. Suzuki (1997), Marine sediments taken during the NH95-1 cruise (in Japanese), in *Preliminary Report of NH95-1*, edited by J. Nishimura, pp. 63–80, Geol. Surv. of Jpn., Natl. Inst. of Adv. Ind. Sci. and Technol., Tsukuba.
- Irino, T., T. Sagawa, Y. Niimura, T. Kanamatsu, T. Yamazaki, and T. Mishima (2003), Lithology of pelagic sediment cores (PC-2, 3, 7) recovered from northwestern Pacific on R/V “Kairei” KR0215 cruise (Japanese with English abstract), *JAMSTEC J. Deep Sea Res.*, *23*, 121–133.
- Karlin, R., and S. Levi (1983), Diagenesis of magnetic minerals in recent hemipelagic sediments, *Nature*, *303*, 327–330.
- Kawahata, H., K. Ohkushi, and Y. Hatakeyama (1999), Comparative late Pleistocene paleoceanographic changes in the midlatitude boreal and austral western Pacific, *J. Oceanogr.*, *55*, 747–761.
- Kirschvink, J. L. (1980), The least-squares line and plane and the analysis of paleomagnetic data, *Geophys. J.R. Astron. Soc.*, *62*, 699–718.
- Laj, C., C. Kissel, A. Mazaud, J. E. T. Channell, and J. Beer (2000), North Atlantic palaeointensity stack since 75 ka (NAPIS-75) and the duration of the Laschamp event, *Philos. Trans. R. Soc. London, Ser. A*, *358*, 1009–1025.
- Lehman, B., C. Laj, C. Kissel, A. Mazaud, M. Paterne, and L. Labeyrie (1996), Relative changes of the geomagnetic field intensity during the last 280 kyr from piston cores in the Azores area, *Phys. Earth Planet. Inter.*, *93*, 269–284.
- Machida, H., and F. Arai (2003), *Atlas of Tephra in and Around Japan* (in Japanese), 336 pp., Univ. of Tokyo Press, Tokyo.
- Maeda, L., H. Kawahata, and M. Nohara (2002), Fluctuation of biogenic and abiogenic sedimentation on the Shatsky Rise in the western North Pacific during the late Quaternary, *Mar. Geol.*, *189*, 197–214.
- McIntyre, A., W. F. Ruddiman, K. Karlin, and A. C. Mix (1989), Surface water response of the equatorial Atlantic Ocean to orbital forcing, *Paleoceanography*, *4*, 19–55.
- Nakanishi, M., K. Tamaki, and K. Kobayashi (1989), Mesozoic magnetic anomaly lineations and seafloor spreading history of the northwestern Pacific, *J. Geophys. Res.*, *94*, 15,437–15,462.
- Nakanishi, M., W. W. Sager, and A. Klaus (1999), Magnetic lineations within Shatsky Rise, northwest Pacific Ocean: Implications for hot spot-triple junction interaction and oceanic plateau formation, *J. Geophys. Res.*, *104*, 7539–7556.
- Oba, T. (1991), The eruption age of the Aso-4 and Ata ashes inferred from oxygen isotope stratigraphy (in Japanese), *Earth Mon.*, *13*, 224–227.
- Oda, H. (2005), Recurrent geomagnetic excursions: A review for the Brunhes normal polarity chron (Japanese with English abstract), *J. Geogr.*, *114*, 174–193.
- Perrin, M., and E. Schnepp (2004), IAGA paleointensity database: Distribution and quality of the data set, *Phys. Earth Planet. Inter.*, *147*, 255–267.
- Rea, D. K. (1994), The paleoclimatic record provided by eolian deposition in the deep sea: The geologic history of wind, *Rev. Geophys.*, *32*, 159–195.
- Sager, W. W., and H. C. Han (1993), Rapid formation of the Shatsky Rise oceanic plateau inferred from its magnetic anomaly, *Nature*, *364*, 610–613.
- Selkin, P. A., and L. Tauxe (2000), Long-term variations in paleointensity, *Philos. Trans. R. Soc. London, Ser. A*, *358*, 1065–1088.
- Stoner, J. S., J. E. T. Channell, C. Hillaire-Marcel, and C. Kissel (2000), Geomagnetic paleointensity and environmental record from Labrador Sea core MD95-024: Global marine sediment and ice core chronostratigraphy for the last 110 kyr, *Earth Planet. Sci. Lett.*, *183*, 161–177.
- Stoner, J. S., C. Laj, J. E. T. Channell, and C. Kissel (2002), South Atlantic and North Atlantic geomagnetic paleointensity stacks (0–80 ka): Implications for inter-hemispheric correlation, *Quat. Sci. Rev.*, *21*, 1141–1151.
- Suganuma, Y., K. Aoki, T. Kanamatsu, and T. Yamazaki (2006), Tephrostratigraphy of deep-sea sediments in the northwestern Pacific and implication for chronology of the past 300 kyr (Japanese with English abstract), *Quat. Res.*, *45*, 435–450.
- Sugiura, N. (1979), ARM, TRM and magnetic interactions: Concentration dependence, *Earth Planet. Sci. Lett.*, *42*, 451–455.
- Tanaka, H., M. Kono, and H. Uchimura (1995), Some global features of paleointensity in geological time, *Geophys. J. Int.*, *120*, 97–102.
- Tanaka, Y. (1997), Marine sediments taken during the NH95-1 cruise (in Japanese), in *Preliminary Report of NH95-1*, edited by A. Nishimura, pp. 138–140, Geol. Surv. of Jpn., Natl. Inst. of Adv. Ind. Sci. and Technol., Tsukuba.
- Tauxe, L. (1993), Sedimentary records of relative paleointensity of the geomagnetic field: Theory and practice, *Rev. Geophys.*, *31*, 319–354.
- Thouveny, N., J. Carcaillet, E. Moreno, G. Leduc, and D. Nerini (2004), Geomagnetic moment variation and paleomagnetic excursions since 400 kyr BP: A stacked record from sedimentary sequences of the Portuguese margin, *Earth Planet. Sci. Lett.*, *219*, 377–396.
- Valet, J. P., L. Meynadier, and Y. Guyodo (2005), Geomagnetic dipole strength and reversal rate over the past two million years, *Nature*, *435*, 802–805.
- Yamazaki, T., and H. Oda (2004), Intensity-inclination correlation for long-term secular variation of the geomagnetic field and its relevance to persistent nondipole components in *Timescales of the Paleomagnetic Field*, *Geophys. Monogr. Ser.*, vol. 145, edited by J. E. T. Channell et al., pp. 287–298, AGU, Washington, D. C.
- Yamamoto, H., and T. Kanamatsu (2002), Lithology of piston cores recovered from continental slope off the east coast of Honshu, Japan on the R/V “Mirai” cruise [MR01-K02] (Japanese with English abstract), *Rep. Jpn. Mar. Sci. Technol. Cent.*, *45*, 7–16.
- Yamamoto, Y. (2006), Possible TCRM acquisition of the Kilauea 1960 lava, Hawaii: Failure of Thellier paleointensity determination inferred

- from equilibrium temperature of the Fe-Ti oxide, *Earth Planet. Space.*, 58, 1033–1044.
- Yamamoto, Y., and H. Tsunakawa (2005), Geomagnetic field intensity during the last 5 Myr: LTD-DHT Shaw palaeointensities from volcanic rocks of the Society Islands, French Polynesia, *Geophys. J. Int.*, 162, 79–114.
- Yamamoto, Y., H. Tsunakawa, and H. Shibuya (2003), Paleointensity study of the Hawaiian 1960 lava: Implications for possible causes of erroneously high intensities, *Geophys. J. Int.*, 153, 263–276.
- Yamazaki, T. (1999), Relative paleointensity of the geomagnetic field during Brunhes Chron recorded in North Pacific deep-sea sediment cores: Orbital influence?, *Earth Planet. Sci. Lett.*, 169, 23–25.
- Yamazaki, T., and N. Ioka (1997), Cautionary note on magnetic grain-size estimation using the ratio of ARM to magnetic susceptibility, *Geophys. Res. Lett.*, 24, 751–754.
- Yamazaki, T., and H. Oda (2005), A geomagnetic paleointensity stack between 0.8 and 3.0 Ma from equatorial Pacific sediment cores, *Geochem. Geophys. Geosyst.*, 6, Q11H20, doi:10.1029/2005GC001001.
- Yamazaki, T., A. L. Abdeldayem, and K. Ikehara (2003), Rock-magnetic changes with reduction diagenesis in Japan Sea sediments and preservation of geomagnetic secular variation in inclination during the last 30,000 years, *Earth Planets Space*, 55, 327–340.
- 
- N. Ioka, The General Environmental Technos Co., Ltd., 1-3-5 Azuchi-cho, Osaka, 541-0052 Japan. (nioka@kanso.co.jp)
- T. Kanamatsu, Institute for Research on Earth Evolution, Japan Agency for Marine-Earth Science and Technology, 2-15 Natsushima-cho, Yokosuka, 237-0061 Japan. (toshiyak@jamstec.go.jp)
- T. Mishima, Center for Advanced Marine Core Research, Kochi University, B200 Monobe, Nankoku, Kochi, 783-8502 Japan. (mishima@cc.kochi-u.ac.jp)
- Y. Yamamoto, Geomagnetism Laboratory, University of Liverpool, Liverpool L69 7ZE, UK. (y.yamamoto@liv.ac.uk)
- T. Yamazaki, Geological Survey of Japan, AIST, Tsukuba, 305-8567 Japan. (toshi-yamazaki@aist.go.jp)